Vítor Hugo Soares Astúcia

Licenciado em Ciências da Engenharia
Electrotécnica e de Computadores

Linear Amplification with Multiple Nonlinear Devices

Dissertação para obtenção do Grau de Mestre em
Engenharia Electrotécnica e Computadores

Orientador : Prof. Doutor Rui Dinis, Professor Auxiliar com Agregação, FCT-UNL

Co-orientador : Prof. Doutor Paulo Montezuma, Professor Auxiliar, FCT-UNL

Júri:

Presidente: Luís Bernardo

Arguente: Francisco Cercas

Vogal: Marco Beko

FACULDADE DE CIÊNCIAS E TECNOLOGIA
UNIVERSIDADE NOVA DE LISBOA

Setembro, 2012

Linear Amplification with Multiple Nonlinear Devices

"It never gets easier, you just get better."

Unknown

Acknowledgements

First of all, I would like to thank my supervisors Prof. Paulo Montezuma and Prof. Rui Dinis who gave me the opportunity to work in this topic and have supported me throughout my thesis with their experience and knowledge.

Also I would like to thank to all colleagues at telecommunication laboratory for their fellowship, great ambience and their advices to overcome all the difficulties during the thesis realization. To my university friends Gonçalo, Vanessa, Raquel, Piscas, Edu, Chalaça, Marcio, Chewbacca, Manta, Pantera, Bola, Marcelo, Zooney, Spread, Rocha who spent with me many days and nights working studding and having fun, without you guys these university time wouldn't be so great. To Anna for all of comprehension, support and encouragement that she always transmitted me.

Last but not least, i would like to thank my family who always believed in me and provided everything possible and necessary to finish my degree. This thesis would certainly not have existed without them. Thanks for the support, motivation and the education that made myself the person that I am today

A special thanks to the Fundação para a Ciência e Tecnologia (FCT) by the financial support through MPSat (PTDC/EEA-TEL/099074/2008) project.

Abstract

In mobile wireless systems, where there are strict power and bandwidth constrains it is desirable to adopt energy efficient constellations combined with powerful equalizer. However, this increased spectral efficiency of multilevel modulations comes at the expense of reduced power efficiency, which is undesirable in systems where power consumption is a constraint. Hence, minimization of the transmitted energy would enable a significant reduction in the total energy consumption of the wireless mobile devices. A simple and practical constellation optimization design would optimize the transmitted energy with a minimum increase in system complexity. The constellation decomposition in terms of a sum of BPSK (Bi-Phase Shift Keying) sub-constellations, relies on an analytical characterization of the mapping rule were the constellation symbols are written as a linear function of the transmitted bits.

Moreover, large constellations in general and non-uniform constellations in particular are very sensitive to interference, namely the residual ISI (Inter-Symbol Interference) at the output of a practical equalizer that does not invert completely the channel effects. IB-DFE (Iterative Block DFE) is a promising iterative frequency domain equalization technique for SC-FDE schemes (Single-Carrier with Frequency Domain Equalization) that allows excellent performance. Therefore it is possible to use the decomposition of constellations on BPSK components to define a pragmatic method for designing IB-DFE receivers that can be employed with any constellation.

In this thesis we consider SC-DFE schemes based on high order M-ary energy optimized constellations with IB-DFE receivers. It is proposed a method for designing the receiver that does not require a significant increase in system complexity and can be used for the computation of the receiver parameters for any constellation. This method is then employed to design iterative receivers, implemented in the frequency-domain, which can cope with higher sensitivity to ISI effects of the constellations resulting from the energy optimization process.

Keywords: Nonlinear amplification, Voronoi, QAM, SC-FDE, IB-DFE, Gain/Phase imbalances

Resumo

Em sistemas de comunicações sem fios onde existe um grande rigor na utilização de largura de banda e potência, é desejável adotar constelações energeticamente eficientes combinadas com equalizadores eficazes. No entanto um aumento de eficiência espectral utilizando constelações multinível leva a um baixo rendimento energético, o que não é desejável em sistemas móveis. Portanto uma redução da energia transmitida permitiria uma redução significativa na energia total consumida pelos dispositivos de comunicação sem fios. Assim a otimização do formato da constelação permitiria a redução da energia transmitida com um incremento mínimo na complexidade do sistema. A decomposição de constelações na soma de sub-constelações BPSK (Bi-Phase Shift Keying), baseia-se numa caracterização analítica de regras de mapeamento onde os símbolos são escritos como uma função linear dos bits transmitidos.

Além disso, grandes constelações em geral e constelações não uniformes em particular, são bastante sensíveis a interferências, nomeadamente o ISI (Inter-Symbol Interference) residual à saída do equalizador que não consegue inverter completamente os efeitos do canal. IB-DFE (Iterative Block DFE) é um equalizador iterativo no domínio da frequência promissor para esquemas SC-FDE (Single-Carrier with Frequency Domain Equalization), que permite excelentes desempenhos. Por isso é possível utilizar uma decomposição de constelações em sub-constelações BPSK para definir um método pragmático de desenho de recetores IB-DFE capazes de lidar com qualquer tipo de constelação.

Nesta tese é considerado um esquema SC-FDE baseado em constelações de grande dimensão e otimizadas energeticamente com um recetor IB-DFE. É proposto um método para desenho do recetor capaz de lidar com qualquer tipo de constelação sem necessitar de um grande aumento de complexidade do sistema. Este método é então utilizado para desenhar recetores iterativos implementados no domínio da frequência que conseguem lidar com a grande sensibilidade aos efeitos do ISI resultantes do processo de otimização de energia.

Palavras-chave: Amplificação não linear, Voronoi, QAM, SC-FDE, IB-DFE, Erros de Fase/Ganho

Contents

List of Acronyms

AWGN Additive White Gaussian Noise

BER Bit Error Rate

BPSK Bi-Phase Shift Keying

CIR Channel Impulse Response

CP Cyclic Prefix

DFE Decision Feedback Equalization

DFT Discrete Fourier Transform

FDE Frequency-Domain Equalization

FFT Fast Fourier Transform

IB-DFE Iterative Block Decision Feedback Equalization

IDFT Inverse Discrete Fourier Transform

ISI Inter-Symbol Interference

LLR Log-Likelihood Ratio

LPF Low-Pass Filter

MC Multi-Carrier

MFB Matched Filter Bound

MMSE Minimum Mean Square Error

MSK Minimun-Shift Keying

OFDM Orthogonal Frequency Division Multiplexing

OPAMP Operational Amplifier

OQAM Offset Quadrature Amplitude Modulation

OQPSK Offset Quadrature Phase Shift Keying

PAM Pulse Amplitude Modulation

PAPR Peak-to-Average Power Ratio

PDP Power Delay Profile

PDF Probability Density Function

PSD Power Spectral Density

QAM Quadrature Amplitude Modulation

QoS Quality of Service

QPSK Quadrature Phase Shift Keying

SC Single-carrier

SC-FDE Single-Carrier with Frequency-Domain Equalization

SER Symbol Error Rate

SINR Signal-to-Interference plus Noise Ratio

SNR Signal-to-Noise Ratio

ZF Zero-Forcing

List of Symbols

a_i	amplitude values from PAM signal
a_n	n^{th} correspondent bits
a_n^p	n^{th} correspondent bits in the parallel format
a_n^s	n^{th} correspondent bits in the series format
a_n^I	n^{th} in-phase correspondent bits
a_n^Q	n^{th} quadrature correspondent bits
b_i	amplitude values from PAM signal
B_k	feedback equalizer coefficient for the k^{th} frequency
$b_n^{(m)}$	m^{th} associated bit to the n^{th} time-domain data symbol (-1 or 1)
$\overline{b}_n^{(m)}$	"hard-decisions" m^{th} associated bit to the n^{th} time-domain data symbol
$b_n^{eq(m)}$	represents $\left(b_n^{(m)}\right)^{\gamma_{m,i}}$
d	minimum Euclidean distance
$d_{\tilde{s}_n,s}$	normalized distance between $\tilde{s}_n$ and s
E_0	energy of minimum amplitude symbol
E_{peak}	peak energy
E_b	average bit energy
E_s	average symbol energy
f_c	carrier frequency
F_k	feedforward equalizer coefficient for the k^{th} frequency
G	gain
G_p	Gray penalty

g_m	m^{th} gain coefficient
H_k	overall channel frequency response for k^{th} frequency
k	frequency index
M	constellation size
N	number of symbols/subcarriers
N_k	channel noise for the k^{th} frequency
N_o	noise power spectral density (unilateral)
$p(t)$	modulation pulse after the match filter
P_b	bit error probability
P_s	symbol error probability
Q	Gaussian tail function
$r(t)$	modulation pulse
r^p	modulation pulse in parallel format
r^s	modulation pulse in series format
$s(t)$	time-domain data symbol
s^I	continuous in-phase component
s^Q	continuous quadrature component
s_i	i^{th} continuous data symbol
$\hat{S_k}$	estimate for k^{th} frequency-domain data symbol
S_k	k^{th} frequency-domain data symbol
$\tilde{S_k}$	"hard-decisions" for k^{th} frequency-domain data symbol
$\overline{S_k}$	"soft-decisions" for k^{th} frequency-domain data symbol
s_n	n^{th} discrete data symbol
s_n^I	discrete in-phase signal component
s_n^Q	discrete quadrature signal component
$\hat{s_n}$	estimate for n^{th} time-domain data symbol
$\tilde{s}_n$	"hard-decisions" for n^{th} time-domain data symbol
$\overline{s_n}$	"soft-decisions" for n^{th} time-domain data symbol
s_n^p	time-domain signal in parallel format
s_n^s	time-domain signal in series format
T	symbol time duration

x^p	modulated signal in parallel format
x^s	modulated signal in series format
x^I	modulated in-phase signal
x^Q	modulated quadrature signal
x_{BP}	transmitted signal
$y(t)$	signal after the match filter
y_k	sampled signal after the match filter
Y_k	received sample for the k^{th} frequency
$\beta_n^{(m)}$	m^{th} associated bit to the n^{th} time-domain data symbol (0 or 1)
Δ	normalized Gilbert distance
$\gamma_{\mu,i}$	binary representation of i
$\lambda_n^{(m)}$	log-likelihood of the m^{th} bit for the n^{th} data symbol
$\mathbf{g}$	gains matrix
$\mathbf{s}$	constellation symbols matrix
$\mathbf{W}$	Hadamard matrix
$\mathfrak{S}$	set of constellation symbols
ϕ_i	i^{th} basis function
$\Psi_i^{(m)}$	subsets of $\mathfrak{S}$ where $\beta_n^{(m)}$ = i
ρ	correlation coefficient
$\rho_n^{(m)}$	correlation coefficient of m^{th} symbol for n^{th} time-domain data symbol
σ_N^2	variance of channel noise
σ_S^2	variance of the transmitted frequency-domain symbols

List of Figures

List of Tables

1

Introduction

In modern wireless mobile communications systems, spectral and power efficiencies are fundamental requirements to assure high data bit rates and maximize the battery duration in mobile devices. The former can be achieved by multilevel modulations. It is well known the ability of high order constellations to improve the spectral efficiency of communication systems. However, this increased spectral efficiency comes at cost of reduced power efficiency, which is undesirable in systems where power consumption can be a main constraint. Hence, the minimization of the transmitted energy would enable a significant reduction in the total energy consumption of the wireless mobile devices. Therefore, designing constellation formats which offer a good trade-off between spectral and power efficiency becomes crucial for efficient battery usage.

On the other hand power amplifiers are also an important part of telecommunication systems, since through amplification we can meet the imposed Quality of Service (QoS) as well as compensate the power loss due to slow fading between transmitter and receiver. In common amplifiers used in mobile communications systems the maximum efficiency is reached near the saturation region. To avoid nonlinear distortion effects, amplifiers are usually over dimensioned which cause losses on power efficiency. So amplifiers may be over dimensioned through power back-off techniques to provide a linear response and avoid non-linear effects that can degrade the signal and reduce the overall system

performance [1].

Nowadays linear amplification is used in telecommunication systems, but this kind of amplification is complex, expensive, and has low efficiency. To achieve the goal of energy efficiency non-linear amplifiers can be used instead. Non-linear amplifiers are more efficient, reduce energy wasting and are simple to implement, which reduce the total cost of system. Still, this is only possible when the signals have constant envelope. On the other hand the better spectral efficiency associated to high order constellations, such as M-Quadrature Amplitude Modulation (QAM), can be assured at cost of higher envelope fluctuations, which make them prone to non-linear effects.

Several techniques can be adopted to reduce envelope fluctuations. For example, M-Offset Quadrature Amplitude Modulation (OQAM) constellations have same spectral efficiency as M-QAM, but lower Peak-to-Average Power Ratio (PAPR), making them more suitable for amplification with non-linear amplifiers. However, despite the reduction on envelope fluctuations, these schemes are not still suitable for amplifiers operating near to the saturation.

1.1 Motivation

Therefore the problem is twofold: maximization of the spectral efficiency and maximization of power efficiency through optimization of constellation's energy and efficient high power amplification. Moreover, large constellations, in general, and non-uniform constellations, in particular, are very sensitive to interference, namely the residual Inter-Symbol Interference (ISI) at the output of a practical equalizer that does not invert completely the channel effects (e.g., a linear equalizer optimized under the Minimum Mean Square Error (MMSE) [2]).

Single-Carrier with Frequency-Domain Equalization (SC-FDE) schemes [3] are excellent candidates for future broadband wireless systems since they can have good performance in severely time-dispersive channels without requiring complex receiver implementation [4, 5]. A promising Iterative Block Decision Feedback Equalization (IB-DFE) approach for SC transmission was proposed in [6] and extended to diversity scenarios [7, 8] and spatial multiplexing schemes [9]. With IB-DFE schemes both the feedforward and the

feedback parts are implemented in the frequency domain. Earlier IB-DFE implementations considered hard decisions (weighted by the blockwise reliability) in the feedback loop. Consequently, theIB-DFE techniques offer much better performances than the non-iterative methods [6, 7]. To improve the performance and to allow truly turbo Frequency-Domain Equalization (FDE) implementations, IB-DFE schemes with soft decisions were proposed[10, 11, 12]. Therefore, we can expect significant performance improvements when we employ IB-DFE receivers with large constellations. However, difficulties may arise in the design of IB-DFE receivers for large constellations, namely on the computation of the reliability of each block, as well as problems on the computation of the average symbol values conditioned to the FDE and/or the channel decoder output.

Another authors have been working in the order to optimize the constellation energy, leading to a constellations with reduced PAPR. However the resultant constellations keep suffering of high sensibility to ISI and high distortion due to non-linear amplifiers working near the saturation point.

Based on the constellation's decomposition as a sum of Bi-Phase Shift Keying (BPSK) sub-constellations it is possible to do an analytical characterization of the mapping rule where the constellation symbols are written as a linear function of the transmitted bits. For that propose we use the analytical method for constellation representation developed in this thesis. Another advantage of the decomposition of high order constellations into BPSK sub-constellations with constant envelope relies on the fact that each sub-constellation can be amplified independently and posteriorly combined to build up the multi-dimensional constellation. Under these conditions it is possible to maximize the efficiency of power amplification operation, since the amplifiers can operate in saturation region without inducing non-linear distortion effects in each amplified signal component.

We consider SC-FDE schemes based on high order M-ary energy optimized constellations with IB-DFE receivers. We propose a method for designing the receiver that does not require a significant increase in system complexity and can be used for the computation of the receiver parameters for any constellation. This method is then employed to design iterative receivers, implemented in the frequency-domain, that can cope with

higher sensitivity to ISI effects of the resulting constellations from the energy optimization process.

1.2 Thesis Structure

In chapter 2 are discussed several aspects regarding the constellations design, energy optimization and analytical characterization of mapping rules. Constellation design and energy optimization problems are characterized in sections 2.2, 2.3 and 2.4. In section 2.5 it is shown that based on the constellation decomposition as a sum of BPSK sub-constellations it is possible to do an analytical characterization of the mapping rule were the constellation symbols are written as a linear function of the transmitted bits.
In chapter 3 are discussed several aspects related with the amplification of generic multi-dimensional constellations. Firstly, sections 3.1 and 3.2 start with the characterization of the amplification problem of Offset Quadrature Phase Shift Keying (OQPSK) constellations, including the analytical characterization of the non-linear effects. Section 3.3 presents a new amplification technique based on the decomposition of multi-dimensional constellations on BPSK components. This also includes the characterization of the structure suitable for the amplification stage. Section 3.4 deals with the matching requirements of the transmitter suitable for parallel amplification structures proposed in section 3.3. The analytical characterization of the impact on performance of phase and gain imbalances between amplifiers is made in the sub-sections 3.4.1 and 3.4.2, where are presented some performance results.
Chapter 4 considers SC-FDE schemes based on high order M-ary energy optimized constellations with IB-DFE receivers. In section 4.1 it is proposed a method to design the receiver that does not require a significant increase in system complexity and can be used for the computation of the receiver parameters for any constellation. Section 4.2 shows that the analytical mapping rule, based on the constellation decomposition as a sum of BPSK sub-constellations, can be applied to the proposed method to extend it into the design iterative receivers, implemented in the frequency-domain, that can cope with higher sensitivity to ISI effects of the constellations resulting from the energy optimization process. Some performance results are presented in section 4.3.

Conclusions and concluding remarks are presented in chapter 5. It also includes future research and complementary topics to the work presented in this thesis.

2

Constellation Design

It is well known the ability of high order modulations to increase spectral efficiency in communication systems. However, this increased spectral efficiency comes at the expense of reduced power efficiency, which is undesirable in systems where power consumption is a constraint. Hence, minimization of the transmitted energy would enable a significant reduction in the total energy consumption of the wireless mobile devices. Therefore, designing constellation formats which offer a good trade-off between spectral and power efficiency becomes crucial for efficient battery usage. In this chapter it will be discussed different approaches to aim an energy optimization of the transmitted signals. In sections 2.1, 2.2 and 2.3 several types of high order modulations are characterized as well as the techniques commonly adopted for energy's optimization. Section 2.4 presents some complementary remarks to the results from previous sections and makes a comparison between the different types of constellations. Finally, section 2.5 presents a new method for analytical characterization of the mapping rules, suitable for Square Quadrature Amplitude Modulation (QAM), Cross-QAM and Voronoi constellations, based on the decomposition of such constellations in Bi-Phase Shift Keying (BPSK) components.

2.1 Square Quadrature Amplitude Modulation

Usually a M-QAM constellation can be written as the sum of two Pulse Amplitude Modulation (PAM) each with dimension $\sqrt{M}$, one for the in-phase (real) component and the other for the quadrature (imaginary) component. The PAM signals are described by $\sum_i a_i r(t - iT)$ and $\sum_i b_i r(t - iT)$, with a_i and b_i real values belonging to an alphabet with size $\sqrt{M}$ and $r(t)$ denoting a rectangular pulse shape with duration T (i.e. symbol duration). Therefore, the corresponding mapping is straightforward: half the bits are used to define the in-phase component (as in the previous case, for Gray mapping or natural binary mapping) and the other half is used to define the quadrature component. This is possible by using orthogonal basis functions to create a final signal as QAM. For instance, in square M-QAM the basis functions associated to in-phase and quadrature components are cosine and sine waves, respectively

$$\phi_1(t) = \sqrt{\frac{2}{T}} \cos(2\pi f_c t), \qquad 0 \leq t \leq T \tag{2.1}$$

$$\phi_2(t) = \sqrt{\frac{2}{T}} \sin(2\pi f_c t), \qquad 0 \leq t \leq T \tag{2.2}$$

where f_c denotes the carrier frequency, and T is the symbol time duration.

To generate a QAM signal two PAM signals are multiplied by the basis functions of (2.1) and (2.2). For example, when $a_i = \pm 1, \pm 3, \pm 5, \pm 7$ and $b_i = \pm 1, \pm 3, \pm 5, \pm 7$ we may have in each component the orthogonal signals shown in Fig.2.1 (in this particular case it is assumed a 8 PAM signal in each component). Under these conditions half of bits are modulated in each component and they can be demodulated independently. Within a i^{th} time symbol interval with duration of T, the resulting M^2-QAM signal is given by

$$s_i(t) = \sqrt{\frac{2E_0}{T}} a_i \cos(2\pi f_c t) + \sqrt{\frac{2E_0}{T}} b_i \sin(2\pi f_c t), \tag{2.3}$$

where E_0 represents energy for a minimum amplitude symbol, and a_i and b_i are amplitude values from PAM signals $\pm\frac{d}{2}, \pm\frac{3d}{2}, ..., \pm\frac{(L-1)d}{2}$, with $L = \sqrt{M}$ and d the minimum Euclidean distance. The signal x_i consists of two quadrature carriers, each one

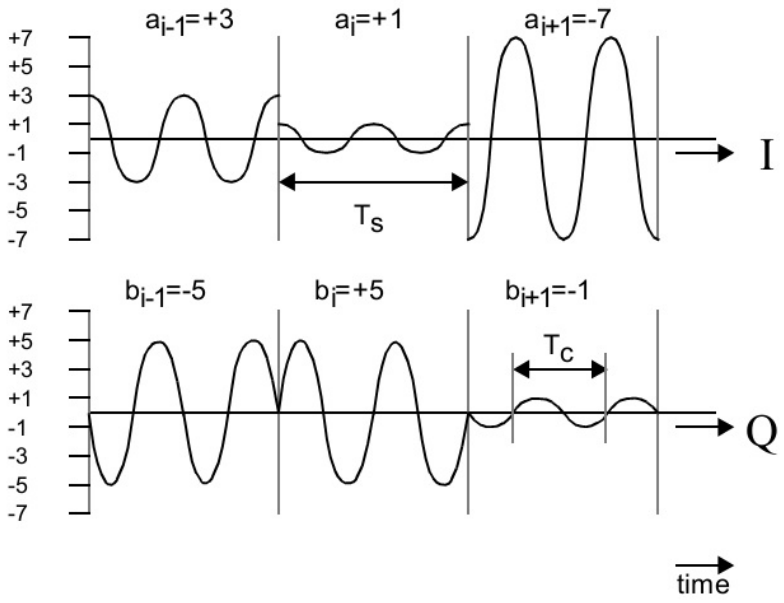

Figure 2.1: Orthogonal signals in Square-QAM.

modulated by a set of discrete amplitudes defined by a_i and b_i. The average symbol energy for square M^2-QAM is given by

$$\begin{aligned} E_s &= \frac{1}{M^2}\sum_{i,j=1}^{M}(s^{I\,2}+s^{Q\,2}) \\ &= d^2\left(\frac{M^2-1}{6}\right). \end{aligned} \tag{2.4}$$

Thus, the average bit energy can be written as

$$E_b = d^2\left(\frac{M^2-1}{6\log_2(M)}\right). \tag{2.5}$$

Therefore, for the minimum Euclidean distance results

$$d = \sqrt{\frac{6\log_2(M)E_b}{M^2-1}}. \tag{2.6}$$

Using the Gilbert approximation [13], we may write the probability of symbol error P_s as

$$P_s \approx NQ(\Delta), \tag{2.7}$$

where N is the average number of adjacent symbols, Q is the Gaussian tail function and

Δ denotes the minimum distance (in signal-to-noise ratio) from a symbol to a decision boundary. From (2.7) and (2.5) and considering a Gray code the Bit Error Rate (BER) can be approximately given by

$$P_b \approx \frac{2}{\log_2(M)}\left(1-\frac{1}{M}\right)Q\left(\sqrt{\frac{6\log_2(M)}{M^2-1}.\frac{E_b}{N_o}}\right), \tag{2.8}$$

where N_0 denotes the one-sided power spectral density of the noise. It becomes clear, that QAM Modulation produces a spectral efficient transmission, however the symbols are very close leading to more errors due to noise and distortions. To overcome these errors more power has to be used in the transmission, and this reduce the power efficiency.

2.2 Cross Quadrature Amplitude Modulation

In the last section we have described how Square-QAM works, but this is valid just when the number of bits is even (i.e., 4-,16-,64-,256-QAM). When the number of bits is odd (i.e, 8-,32-,128-QAM), rectangular constellations are not the best choice, as it is shown in [13]. To reduce the peak and average power, a Cross-QAM is used instead of Square-QAM. Cross-QAM constellations started being used in schemes where the constellation size change with the channel quality. Contrarily to Square-QAM ($M = 2^m$) where the changes on size are from m to $m+2$ (the constellations sizes are power of 4, i. e. 16 to 64 to 256-QAM and so on), with Cross-QAM modulation the increase on size is smoother, we may pass from m to $m+1$. Cross-QAM constellations based on a symmetric pattern assure three performance parameter improvements associated with a symmetric pattern: 1) reduced average symbol signal-to-noise ratio; 2) a smaller peak power requirement; 3) a lower signal set dynamic range. To generate a Cross-QAM constellation of m bits, we start with a square constellation of $m-1$ bits, then each side is extended by 2^{m-3} symbols as shown in Fig. 2.2 [13]. The corners should be ignored because these areas require more power to amplify [14]. In Cross-QAM constellations a pure Gray code is not applicable, therefore the BER has some increment related with number of different bits between adjacent symbols. Recall that rectangular M-QAM constellations may have a bit-symbol correspondence that yields exactly one-bit differences in bit representations of adjacent

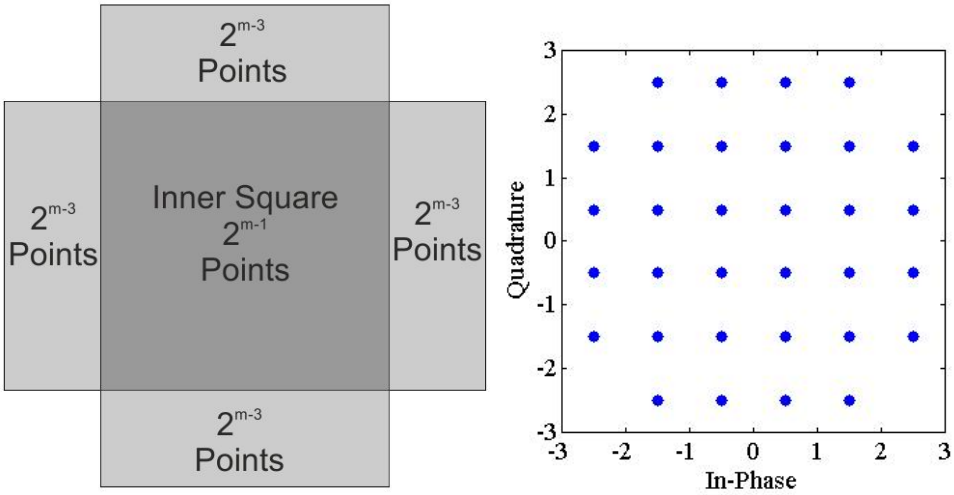

Figure 2.2: Illustrating how to obtain a Cross-QAM from Square-QAM.

symbols, i.e., a "pure" Gray code. On the other hand Cross-QAM and Voronoi constellations have "impure Gray codes" where the reflected binary property of Gray codes does not holds, since any two equidistant symbols from a particular bit change do not differ only in that bit. Consequently, they suffer a "Gray code penalty", G_p, i.e. the average number of bit differences per adjacent decision region (for pure Gray this value is near unity [13]). Thus, on the average, a single symbol threshold error will cause G_p bits to be in error.

The "peak Gray penalty" G_p is defined as the maximum (over the constellation) number of bit-errors per single symbol threshold error. Thus the BER suffers an increment represented by Gray penalty (usually this factor have values near 1), leading to

$$P_b \cong \frac{G_p N}{\log_2(M)} Q(\Delta), \tag{2.9}$$

where Δ, denotes the normalized "Gilbert distance" of the array, is the least distance (in signal-to-noise ratio) from a signal point to a decision boundary. N represents the "Gilbert number" of the constellation and it is the average (over the array) number of distinct" decision boundaries exactly at distance Δ from a signal point. N may be thought of as the average number of "nearest neighbours" in the constellation, since a decision boundary at the minimum distance Δ implies another signal point equidistant beyond it.

From [15] and assuming equally probable symbols, we may write the minimum Euclidean distance as

$$d = \sqrt{\frac{48\log_2(M)E_b}{31M-32}}. \tag{2.10}$$

For $M \geq 32$, N is given by $\left(4 - \frac{6}{\sqrt{2M}}\right)$ thereby is valid to approximate the BER by

$$P_b \cong \frac{G_p}{\log_2(M)}\left(4 - \frac{6}{\sqrt{2M}}\right)Q\left(\sqrt{\frac{48\log_2(M)}{31M-32}.\frac{E_b}{N_o}}\right). \tag{2.11}$$

Contrarily to Square-QAM, it is not straightforward the decomposition of this constellation into PAM signals. So it can be not possible to split in In-Phase and Orthogonal components and compute independently the transmitted bits in each component.

2.3 Voronoi constellations

As referred before the energy optimization of any constellation can reduce the transmitted power. Of course it is not possible such optimization with square or cross-QAM constellations. To reduce the transmitted power, different methodologies have been adopted for the design of constellations shapes. One approach is to resort to lattice codes, which have been extensively used in the definition of multilevel modulation formats for Additive White Gaussian Noise (AWGN) channels [16, 17]. Another approach minimizes the average power through constellation shaping and non equiprobable signalling [16, 18]. The former is done by selecting the set of points in a lattice which have minimum energies, whereas the latter minimizes the average power by reducing the transmission frequency of points with high energies. In addition, by numerical optimization techniques it is possible to find the best possible packing of constellation points as in [19] for different power constrains, whether average or peak power.

In conclusion, we may say that the optimization problem relies on the identification of the constellation shape that provides the densest configuration of the constellations points, which is not a trivial problem and the solution requires a mathematical optimization process. The *kissing problem* is a good approach to this problem, which is a basic geometric problem that asks how many balls, with the same size, can touch one given ball at the

same time. The answer for this problem is six balls, representing a hexagonal shape, as shown in Fig. 2.3 [20].

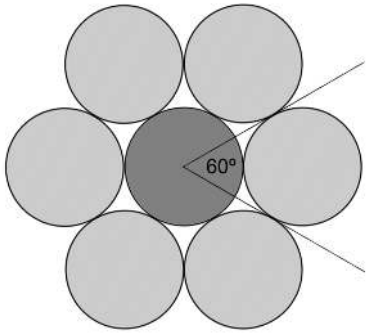

Figure 2.3: Kissing arrangement for R^2

For a 2-dimensional Euclidean space $\Re^2$ it can be shown that Voronoi region have hexagonal shape which corresponds the densest region disposition. Under this configuration we have the optimum average Euclidean distance between symbols, with them placed over a hexagonal lattice with a unit minimum separation given by [21].

$$min\left(\frac{1}{M}\sum_{i=0}^{M-1}|s_i|^2\right), \quad subject\ \ to, \quad d^2(s_i,s_j)_{i\neq j} \geq 1. \tag{2.12}$$

It should be mentioned that Voronoi codes only attain certain rates and since the shaped regions defining them are not circular, they do not have in general the lowest possible energy (although for 2-dimensional Euclidean real space the difference to the minimum energy configuration is small). Obviously, due to the lower transmitted energy, Voronoi constellations can achieve performance improvements over Square and Cross-QAM.

Examples of optimal Voronoi constellations with sizes of 16, 32 and 64 are shown in Fig.2.4. It can be seen the higher density of the resulting constellations, since the symbols are now packed in a smaller area when compared with rectangular or Cross-QAM constellations with the same size. That is, the performance improvement is achieved because the area occupied by symbols are smaller than QAM, requiring less transmitted energy for the same number of points. This improvement grows with the constellations size but at cost of increase in the receiver complexity. Similarly to Cross-QAM, due to the higher number of adjacent symbols, these constellations do not have pure Gray code, being the

BER affected by a Gray code penalty. However, and despite this degradation factor for high values of Signal-to-Noise Ratio (SNR) the performance of Voronoi constellations overpass performance of other constellations (Square QAM and Cross-QAM).

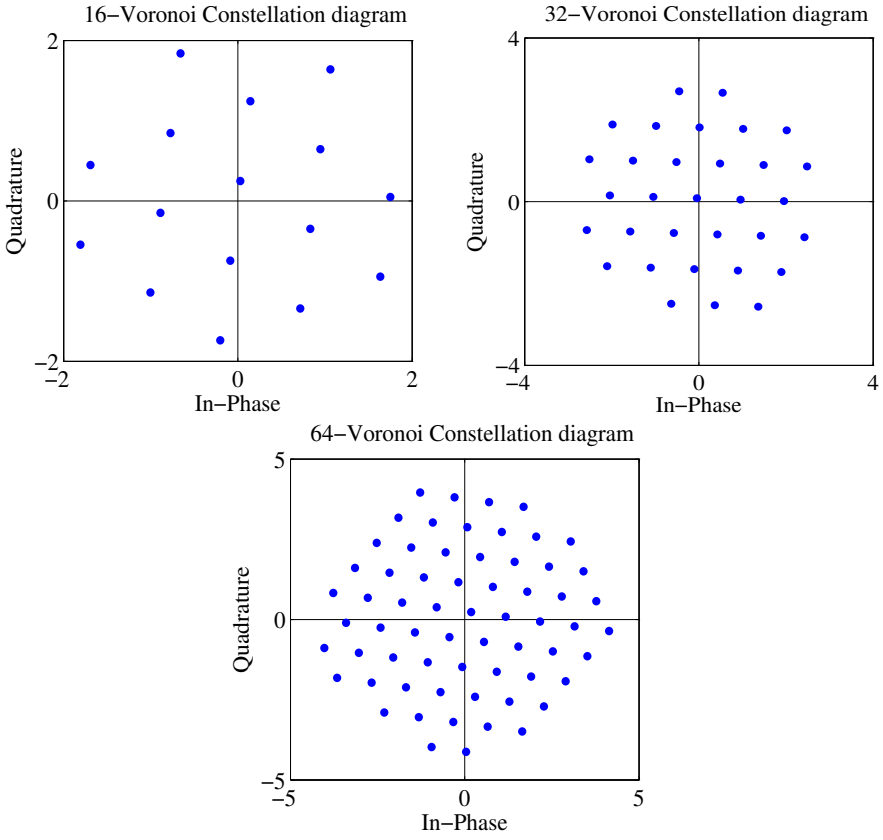

Figure 2.4: Optimized energy Voronoi constellations for 16, 32 and 64 symbols

2.4 Comparison Between Constellations

For comparison purposes we consider the three types of constellations from previous sections. Several parameters should be taken into account, as the number of adjacent symbols, the coding rule, the Peak-to-Average Power Ratio (PAPR) and the energy gains of each one. It should be mentioned that the constellation shape together with the number of adjacent symbols have direct impact in the shape of the decision regions. For instance, contrarily to Square QAM in non uniform constellations the shape of the decision regions it is not the same for all. This fact can have impact in receiver's complexity.

On the other hand a pure Gray code it is only possible with Square-QAM constellation. Due to the relation (bits/adjacent symbols) Cross-QAM and Voronoi constellations do

not support a pure Gray code, which affects the performance for low SNR values. Nevertheless Cross-QAM has the ability to take Gray code with some gap as shown in section 2.2.

Regarding the energy optimization, two parameters must be compared: the energy gain over an Quadrature Phase Shift Keying (QPSK) constellation and the PAPR. We will consider as reference a QPSK constellation which has a average bit energy given by the follow expression,

$$E_{b_{(QPSK)}} = \frac{d^2}{4}. \tag{2.13}$$

Therefore, we may define the energy gain G as,

$$G = \frac{E_{b_{(QAM,VOR)}}}{E_{b_{(QPSK)}}}. \tag{2.14}$$

Due to the number of symbols, the considered constellations need more energy in the transmission than QPSK, (in table 2.2 we can see negative gains). It means for transmit the given constellations is needed more power than to transmit QPSK constellation, as was expected.

Voronoi and Square QAM constellations are characterized by the values of energy gains and average number of adjacent symbols shown in table 2.1 and table 2.2, respectively. As we can see from table 2.2, when compared with QAM constellations, Voronoi constellations have energy gains of 0.6 dB, 0.38 dB and 0.75 dB for 16, 32 and 64 symbols, respectively. So it is clear that Voronoi constellations have higher gains, i.e. Voronoi constellations can achieve the same bit error rate as QAM using less transmitted energy per bit. At same time, these higher energy gains are associated to an higher number of adjacent symbols (see table 2.1), which can compromise the performance outside the asymptotic zone, i. e. for low values of SNR. Consequently, the receiver must take into account this effect as well as the expected increase on the sensitivity of the resulting non uniform constellations to Inter-Symbol Interference (ISI).

In a real amplification system, it is convenient to limit the dynamic range of the input signal to avoid operation in the saturation zone. This is special valid for the peak power

Table 2.1: Average number of adjacent symbols

Constellation type \ size	**16**	**32**	**64**
QAM	3	3.25	3.5
Voronoi	4.12	4.68	5.09

Table 2.2: Energy gains(dB)(reference QPSK constellation)

Constellation type \ size	**16**	**32**	**64**
QAM	-3.98	-5.91	-8,45
Voronoi	-3.40	-5.46	-7.69

of the input signal. For signals with high values of PAPR, the amplifiers can be saturated for part of the dynamic range of the input signal, leading to non linear effects. As referred before, over dimensioning the amplifier can be one solution to avoid the non linear distortion, but compromises the amplification efficiency. Another solution can be the reduction of the PAPR, since signals with lower PAPR have lower dynamic range and are less sensitive to non linear amplifiers' effects. Therefore, PAPR is crucial to evaluate the immunity of each constellation against non linear effects, which may affect the overall efficiency of an amplification process [22].

From the definition the Peak Energy is,

$$E_{peak} = max_i \sum_{n=0}^{M-1} s_{i,n}^2. \tag{2.15}$$

From (2.15), the PAPR is given by

$$PAPR = \frac{E_{peak}}{E_s}. \tag{2.16}$$

As we can see in Table 2.3, due to the densest symbols in Voronoi constellations, they have lower energy and better PAPR than Square-QAM constellations. Although, there is an exception for constellations with 32 symbols, since in this case lower energy Voronoi constellations do not assure lower PAPR than Cross-QAM constellations.

Table 2.3: PAPR values for Voronoi and QAM constellations

Constellation type / size	16			32			64		
	E_{peak}	E_s	$PAPR$	E_{peak}	E_s	$PAPR$	E_{peak}	E_s	$PAPR$
QAM	4.50	2.50	1.80	8.50	5.00	1.70	24.50	10.50	2.33
Voronoi	3.81	2.19	1.74	8.45	4.40	1.92	17.28	8.82	1.96

2.5 General Constellation Mapping

General Mapping

Previous improvements on constellations energy efficiency are achieved with a significant increase in system complexity due to the complex nature of the bit sequence-to-signal mappings. Hence, besides a simple and practical constellation optimization design that would optimize the transmitted energy it is also desirable a simple method for analytical characterization of the resulting mapping rule, where the constellation symbols are written as a linear function of the transmitted bits. It can be shown [23] that the constellation symbols can be expressed as function of the corresponding bits as follows [1]:

$$\begin{aligned} s_n &= g_0 + g_1 b_n^{(1)} + g_2 b_n^{(2)} + g_3 b_n^{(1)} b_n^{(2)} + g_4 b_n^{(3)} + ... \\ &= \sum_{i=0}^{M-1} g_i \prod_{m=1}^{\mu} \left(b_n^{(m)} \right)^{\gamma_{m,i}}, \end{aligned} \tag{2.17}$$

for each $s_n \in \mathfrak{S}$, where $(\gamma_{\mu,i} \ \gamma_{\mu-1,i} \ ... \ \gamma_{2,i} \ \gamma_{1,i})$ is the binary representation of i and $b_n^{(m)} = 2\beta_n^{(m)} - 1$ (throughout this thesis we assume that $\beta_n^{(m)}$ is the mth bit associated to the nth symbol and $b_n^{(m)}$ is the corresponding polar representation, i.e., $\beta_n^{(m)} = 0$ or 1 and $b_n^{(m)} = -1$ or +1, respectively). Since we have M constellation symbols in $\mathfrak{S}$ and M complex coefficients g_i, (2.17) is a system of M equations that can be used to obtain the coefficients g_i, $i = 0, 1, ..., \mu - 1$. Writing (2.17) in matrix format we have

$$\mathbf{s} = \mathbf{W}\mathbf{g}, \tag{2.18}$$

[1] It should be noted that in this subsection s_n denotes the nth constellation point but in the previous section s_n denotes the nth transmitted symbol; the same applies to $b_n^{(m)}$ (or $\beta_n^{(m)}$) that here denotes the mth bit of the n constellation point (instead of the mth bit of the nth transmitted symbol)

with

$$\mathbf{s} = [s_1 \; s_2 \; ... \; s_M]^T, \tag{2.19}$$

$$\mathbf{g} = [g_0 \; g_1 \; ... \; g_{\mu-1}]^T, \tag{2.20}$$

and $\mathbf{W}$ is a Hadamard matrix with dimensions $M \times M$. Clearly, the vector of constellation points $\mathbf{s}$ is the Hadamard transform of the vector of coefficients $\mathbf{g}$. Therefore, for a given constellation we can obtain the corresponding coefficients g_i from the inverse Hadamard transform of the vector of constellation points. The Hadamard matrix is computed from the relation $\mathbf{W} = 2\mathbf{W}' - 1$ where $\mathbf{W}'$ is a matrix given by

$$\begin{bmatrix}
1 & 1 & 1 & 1 & 1 & 1 & 1 & 1 & 1 & 1 & 1 & 1 & 1 & 1 & 1 & 1 \\
1 & 0 & 1 & 0 & 1 & 0 & 1 & 0 & 1 & 0 & 1 & 0 & 1 & 0 & 1 & 0 \\
1 & 1 & 0 & 0 & 1 & 1 & 0 & 0 & 1 & 1 & 0 & 0 & 1 & 1 & 0 & 0 \\
1 & 0 & 0 & 1 & 1 & 0 & 0 & 1 & 1 & 0 & 0 & 1 & 1 & 0 & 0 & 1 \\
1 & 1 & 1 & 1 & 0 & 0 & 0 & 0 & 1 & 1 & 1 & 1 & 0 & 0 & 0 & 0 \\
1 & 0 & 1 & 0 & 0 & 1 & 0 & 1 & 1 & 0 & 1 & 0 & 0 & 1 & 0 & 1 \\
1 & 1 & 0 & 0 & 0 & 0 & 1 & 1 & 1 & 1 & 0 & 0 & 0 & 0 & 1 & 1 \\
1 & 0 & 0 & 1 & 0 & 1 & 1 & 0 & 1 & 0 & 0 & 1 & 0 & 1 & 0 & 0 \\
1 & 1 & 1 & 1 & 1 & 1 & 1 & 1 & 0 & 0 & 0 & 0 & 0 & 0 & 0 & 0 \\
1 & 0 & 1 & 0 & 1 & 0 & 1 & 0 & 0 & 1 & 0 & 1 & 0 & 1 & 0 & 1 \\
1 & 1 & 0 & 0 & 1 & 1 & 0 & 0 & 0 & 0 & 1 & 1 & 0 & 0 & 1 & 1 \\
1 & 0 & 0 & 1 & 1 & 0 & 0 & 1 & 0 & 1 & 1 & 0 & 0 & 1 & 1 & 0 \\
1 & 1 & 1 & 1 & 0 & 0 & 0 & 0 & 0 & 0 & 0 & 0 & 1 & 1 & 1 & 1 \\
1 & 0 & 1 & 0 & 0 & 1 & 0 & 1 & 0 & 1 & 0 & 1 & 1 & 0 & 1 & 0 \\
1 & 1 & 0 & 0 & 0 & 0 & 1 & 1 & 0 & 0 & 1 & 1 & 1 & 1 & 0 & 0 \\
1 & 0 & 0 & 1 & 0 & 1 & 1 & 0 & 0 & 1 & 1 & 0 & 1 & 0 & 0 & 1
\end{bmatrix}, \tag{2.21}$$

As stated previously, a M-QAM constellation can be written as a sum of two PAM each with dimension $\sqrt{M}$, one for the in-phase (real) component and the other for the quadrature (imaginary) component. Therefore, the corresponding mapping is straightforward:

half the bits are used to define the in-phase component (with Gray mapping or natural binary mapping) and the other half is used to define the quadrature component. Another possibility is to represent any M-QAM constellations as a sum of BPSK sub-constellations[24]. For instance, the constellations 16 and 32 QAM can be decomposed in a sum of BPSK signals with the mapping rule defined by the set of non null complex coefficients $g_2 = 2j$, $g_3 = j$, $g_8 = 2$, $g_{12} = 1$ and $g_2 = 1.375j$, $g_3 = 0.375j$,$g_6 = 0.375j$, $g_7 = -0.125j$, $g_{10} = 0.375j$, $g_{11} = -0.125j$, $g_{14} = 0.375j$, $g_{15} = -0.125j$, $g_{16} = -1.375$, $g_{17} = -0.125$, $g_{20} = 0.625$, $g_{21} = -0.125$, $g_{24} = -0.375$, $g_{25} = -0.125$, $g_{28} = 0.125$, $g_{29} = -0.125$, respectively.

On the other hand, in Voronoi constellations the mapping rules are those that assure an energy optimization. For example, the Voronoi constellation with 16 symbols is characterized by the set of complex coefficients $g_0 = 0$, $g_1 = -0.58 + j0.57$, $g_2 = -0.712 + j0.545$, $g_3 = -0.014 - j0.124$, $g_4 = 0.028 + j0.248$, $g_5 = -0.186 + j0.273$, $g_6 = -0.2 + j0.149$, $g_7 = -0.014 - j0.124$, $g_8 = -0.1 + j0.074$, $g_9 = 0.085 - j0.198$, $g_{10} = 0.358 + j0.272$, $g_{11} = 0.859 - j0.198$, $g_{12} = -0.1 + j0.074$, $g_{13} = -0.085 - j0.198$, $g_{14} = -0.1 + j0.074$ and $g_{15} = 0.085 - j0.198$, which corresponds to the constellation symbols shown in Fig.2.4. For a dimension of 32 we have the sets of complex coefficients $g_0 = 0$, $g_1 = -0.848 - j0.328$, $g_2 = 0.136 - j0.140$, $g_3 = 0.147 + j0.184$, $g_4 = 0.426 + j0.120$, $g_5 = -0.342 - j0.394$, $g_6 = -0.048 - j0.025$, $g_7 = 0.007 - j0.244$, $g_8 = -0.271 + j0.741$, $g_9 = 0.026 + j0.297$, $g_{10} = 0.040 - j0.191$, $g_{11} = 0.411 - j0.312$, $g_{12} = 0.022 + j0.189$, $g_{13} = -0.122 - j0.348$, $g_{14}0.048 + j0.025 =$, $g_{15} = 0.095 - j0.410$, $g_{16} = -0.280 - j0.396$, $g_{17} = -0.327 + j0.039$, $g_{18} = 0.011 - j0.136$, $g_{19} = 0.140 - j0.032$, $g_{20} = -0.007 + j0.244$, $g_{21} = 0.474 - j0.314$, $g_{22} = -0.313 - j0.449$, $g_{23} = -0.243 - j0.235$, $g_{24} = 0.022 + j0.189$, $g_{25} = -0.048 - j0.025$, $g_{26} = 0.048 + j0.025$, $g_{27} = -0.213 - j0.290$, $g_{28} = 0.206 + j0.074$, $g_{29} = -0.173 - j0.021$, $g_{30} = -0.085 - j0.187$, $g_{31} = -0.272 - j0.180$.

It should be mentioned that, due to energy optimization for both constellations types, the resulting mapping rule for M-QAM constellations corresponds to the optimal mapping of bits that minimizes the average number of different bits between one symbol and his neighbours.

Based on the constellations decomposition as a sum of BPSK sub-constellations it is possible to provide an analytical characterization of the mapping rule were the constellation

symbols are written as a linear function of the transmitted bits. This method is then employed to design iterative receivers, implemented in the frequency-domain, that can cope with higher sensitivity to ISI effects of the constellations resulting from the energy optimization process.

3

Efficient Amplification for General Constellations

Typically power amplifiers are an important part in a telecommunication system, they are responsible for amplify the signal in transmitter till the level needed to overcome the loss between transmitter and receiver. A dependency of linear amplifiers makes the transmitter amplification non-efficient, because they exhibit non-linear behaviours when operating close to saturation region. So linear amplifiers must have some power backed off techniques to provide a linear response, once the non-linear effects eventually degrade the signal and reduce the system performance [1]. Linear amplification with non-linear amplifiers take advantage from saturation region to improve the energy efficiency, but these amplifiers can only be used if the signal has constant envelope. Let's consider the following signal which has constant envelope.

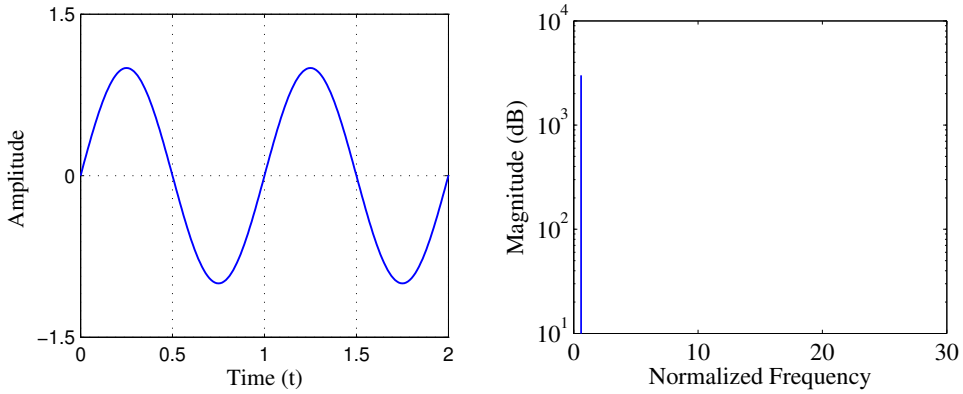

Figure 3.1: Sin wave with constant envelope and Power Spectral Density (PSD)

Amplifying this signal with the saturated amplifier as a Operational Amplifier (OPAMP) the resultant signal would be similar to Figure 3.2

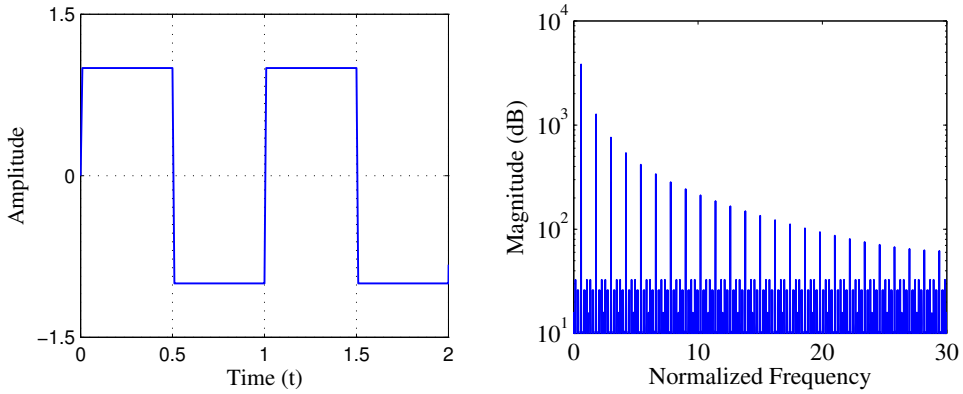

Figure 3.2: Rect signal and PSD

With the amplifier designed to work in the frequency of fundamental harmonic, the remaining harmonics are filtered so we have the original signal at the amplifier output. The constant envelope signal doesn't lose any information when is amplified by a non-linear amplifier, because the whole information is contained in the first and single harmonic, this is the motivation for the follow demonstration.

The modulations schemes having low envelope fluctuation are often recommended for digital transmission whenever non-linear amplifiers are used, namely in the mobile and satellite communications. The most common modulations which ensure a constant envelope or at least quasi-constant envelope are Offset Quadrature Phase Shift Keying

(OQPSK) and Minimun-Shift Keying (MSK) modulations schemes. These schemes more than constant envelope, exhibit a compact spectrum and high detection efficiency, archived with simple receivers [12].

In the last chapter was shown how constellations are expressed as function of the corresponding bits. Now we will take advantage of this method to achieve the efficient amplification of general constellations.

3.1 Parallel and Series OQPSK Signals

A OQPSK signal can be written as,

$$x^p(t) = \sum_{n=0}^{N-1} a_n^I r^p(t - n2T) + j \sum_{n=1}^{N-1} a_n^Q r^p(t - 2nT - T) \tag{3.1}$$

where $r(t)$ is the modulation pulse and $2T$ represents the bit duration. The coefficients $a_n^I = \pm 1$ and $a_n^Q = \pm 1$ are respectively, the nth in-phase and quadrature bits [25].

The in-phase and quadrature data streams are shifted in the time domain half bit (T), this shift limits the carrier phase shift. If a_n^I or a_n^Q changes sign, a phase shift of $\pm 90^o$ occurs. If both carriers can change only once ever 2T and a sign change occurs in both during the same period results in a 180^o phase shift. In OQPSK, in-phase and quadrature carriers cannot change the phase simultaneously. One carrier has transitions in the middle of the other symbol, this way eliminates the 180^o phase changes.

We can write OQPSK in the parallel format as

$$x^p(t) = \sum_{n=0}^{N-1} a_n^p r^p(t - nT), \tag{3.2}$$

where

$$a_n^p = \begin{cases} a_{n'}^I & n' = 2n \\ j a_{(n')}^Q & n' = 2n + 1 \end{cases} \tag{3.3}$$

It should be noted that symbols are spaced by T and they have alternately real and imaginary values, i.e. $\{a_n^p\} = \{a_0^I | j a_0^Q | a_1^I | j a_1^Q | ... | a_{n-1}^I | j a_{n-1}^Q\} = \{\pm 1 | \pm j | \pm 1 | \pm j | ... | \pm 1 | \pm j\}$.

For a Quadrature Phase Shift Keying (QPSK) scheme a transmitted signal is given by

$$x_{BP}(t) = Re\{x^p(t)exp(j2\pi f_c t)\} = x^I(t)cos(2\pi f_c t) - x^Q(t)sin(2\pi f_c t), \tag{3.4}$$

where f_c is the carrier frequency and x^p is its complex envelope given by (3.2). The previous equation can be written in this format

$$x_{BP}(t) = Re\left\{x^p(t)exp\left(j\frac{\pi t}{2T}\right)exp\left(j2\pi\left(f_c - \frac{1}{4T}\right)t\right)\right\}. \tag{3.5}$$

We may define the complex envelope relatively to $f_c^{\shortmid} = f_c - \frac{1}{4T}$ and, $x^s(t) = x^p(t)exp\left(j\frac{\pi t}{2T}\right)$ [26]. Consequently (3.5) is given by

$$x_{BP}(t) = Re\left\{x^s(t)exp(j2\pi f_c^{\shortmid} t)\right\}. \tag{3.6}$$

From (3.2) we may write a OQPSK series signal as[1]

$$x^s(t) = \sum_{n=0}^{N-1} a_n^s r^s(t - nT), \tag{3.7}$$

considering a complex modulation pulse

$$r^s(t) = r^p(t)exp\left(j\frac{\pi t}{2T}\right), \tag{3.8}$$

and

$$a_n^s = a_n^p(-j)^{2n}. \tag{3.9}$$

The last equation can take the following values

$$a_n^s = \begin{cases} a_{2n}^s = a_{2n}^p(-j)^{2n} = a_n^I(-1)^n = \pm 1 \\ a_{2n+1}^s = a_{2n+1}^p(-j)^{2n+1} = a_n^Q(-1)^n = \pm 1 \end{cases} \tag{3.10}$$

A OQPSK series bit stream can be seen as a Bi-Phase Shift Keying (BPSK) stream where the even and odd bits are respectively in-phase and quadrature bits. So the OQPSK series

[1] with $t = nT$, $exp(j\frac{\pi t}{2T}) = j^n$

can be regarded as a BPSK modulation with a complex modulation pulse.

3.2 Efficient Modulation Pulse

In the last section we were presenting the OQPSK signal in the serial and parallel format. The MSK signal can be seen as a OQPSK signal which has a different modulation pulse $r(t)$. The OQPSK signal defined in (3.2) with the $r(t) = rect(\frac{t}{2T})$ has some envelope fluctuation as we can see by the I-Q diagram in Figure 3.3. These fluctuations can cause severe non-linear distortions on the transmitted signal, so a MSK scheme can be used to overcome these effects.

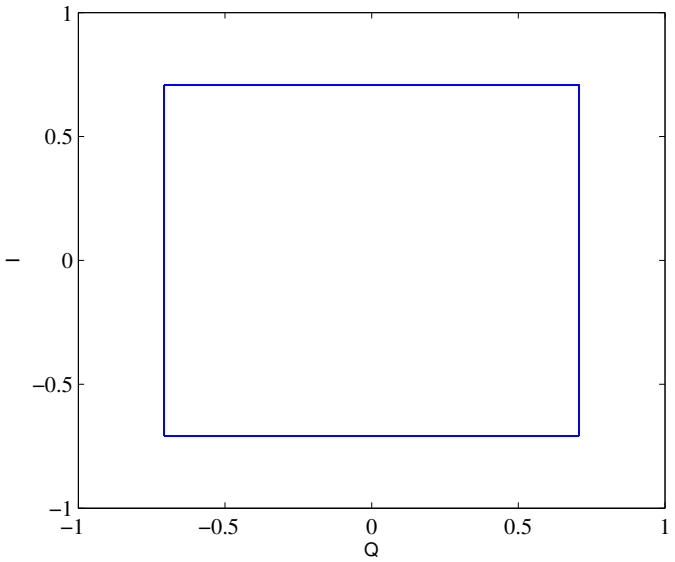

Figure 3.3: OQPSK I-Q diagram

A MSK signal is given by

$$x(t) = \sum_{n=0}^{N-1} a_n r(t - nT), \tag{3.11}$$

where the pulse shape is $r(t) = cos\left(\frac{\pi t}{2T}\right) rect\left(\frac{t}{2T}\right)$. Using a half cosine pulse leads to a constant envelope signal as depicted in the I-Q diagram Figure 3.4. Thereby this little envelope fluctuations from the OQPSK scheme which could degrade the signal after the non-linear amplifier are vanished. For the non-linear amplification is a important

behaviour

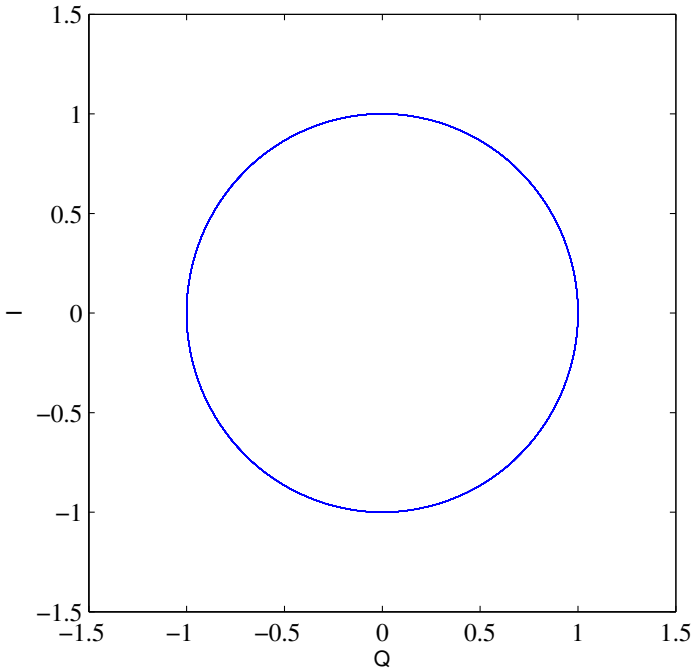

Figure 3.4: MSK I-Q diagram

3.3 General Constellations Amplification

As seen in the previous chapter, Quadrature Amplitude Modulation (QAM) and Voronoi constellation can be expressed as a sum of OQPSK signals (2.17). In this section will be introduced a serial approach for these constellations. It takes into account the series approach presented in the last section for OQPSK signal.

Let us define in this chapter s_n as

$$s_n = \sum_{m=0}^{M-1} g_m b_n^{eq(m)}, \tag{3.12}$$

with $b_n^{eq(m)} = \prod_{m=1}^{\mu} \left(b_n^{(m)} \right)^{\gamma_{m,i}}$, thereby $b_n^{eq(1)} = 1$; $b_n^{eq(2)} = b_n^0$; $b_n^{eq(3)} = b_n^1$; $b_n^{eq(4)} = b_n^0 b_n^1$; etc. This reduction is just to make the notation clear.

We can express s_n in the quadrature and in-phase components, each component represents a BPSK signal.

$$s_n = s_n^I + j s_n^Q, \tag{3.13}$$

where

$$s_n^I = \sum_{m=0}^{M-1} Re\{g_m\} b_n^{eq(m)} \tag{3.14}$$

$$s_n^Q = \sum_{m=0}^{M-1} Im\{g_m\} b_n^{eq(m)} \tag{3.15}$$

b_n^{eq} represents the phase(± 1) from the correspondent bits and g_m the signal amplitude gain. From (3.1) and (3.13) QAM and Voronoi signals in the parallel format are written as

$$\begin{aligned} x^p(t) &= \sum_{n=0}^{N-1}\sum_{m=0}^{M-1} Re\{g_m\} b_n^{eq(m)} r^p(t-n2T) + j\sum_{n=1}^{N-1}\sum_{m=0}^{M-1} Im\{g_m\} b_n^{eq(m)} r^p(t-2nT-T) \\ &= \sum_{n=0}^{N-1} s_n^I r^p(t-n2T) + j\sum_{n=1}^{N-1} s_n^Q r^p(t-2nT-T) \qquad (3.16) \\ &= \sum_{n=0}^{N-1} s_n^P r^p(t-nT) \qquad (3.17) \end{aligned}$$

with

$$s_n^p = \begin{cases} s_{2n}^I \\ j s_{(2n+1)}^Q \end{cases} \tag{3.18}$$

Extending the OQPSK series properties from section 3.1 and shifting the reference carrier from f_c to $f_c^{\shortmid} = f_c - \dfrac{1}{4T}$, the series format for QAM and Voronoi constellations is given by

$$x^s(t) = \sum_{n=0}^{N-1} s_n^s r^s(t-nT), \tag{3.19}$$

where $r^s(t) = r^p(t) exp\left(j\dfrac{\pi t}{2T}\right)$ and $s_n^s = a_s^p(-j)^n$. Now every s_n component can be regarded as a BPSK signal, which can be amplified by a high non-linear amplifier, i.e this signal can be sent to a power amplifier as a OPAMP working in the saturation zone which has high power efficiency. We can see that for each N data block transmitted $\{s_n^s\}$

are alternately the in-phase and quadrature values as shown in (3.20)

$$\{s_n^s\} = \{+s_0^I| - s_0^Q| - s_1^I| + s_1^Q| + s_2^I| - s_2^Q| - s_3^I| + s_3^Q|...| \pm s_{n-1}^I| \pm s_{n-1}^Q\}. \tag{3.20}$$

The transmitter structure we are considering is depicted in the Figure 3.5

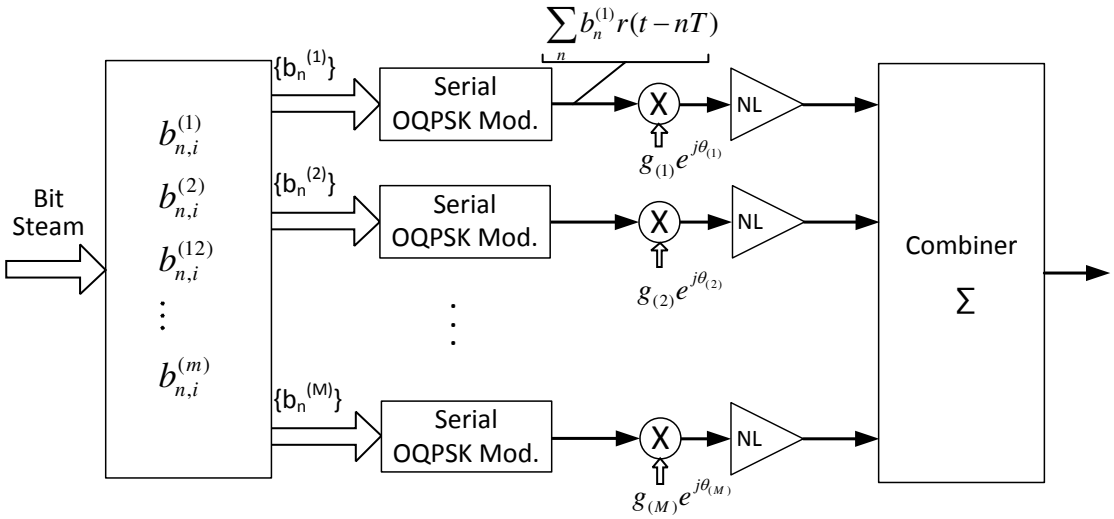

Figure 3.5: General transmitter structure

As shown in the transmitter structure the first block transforms a $\{b_n^{(i)}\}$ bit sequence in μ set of signals b_n^{eq}, once again $\mu = log_2(M)$. Then each b_n^{eq} is multiplied by the complex modulation pulse $r(t)$ and individually amplified. To obtain a amplified signal, whole set of s_n^s signals are linearly combined by the last block to build the x_n^s signal.

3.4 Matching Requirements

In the last section was shown the transmitter structure which takes advantage from the high efficiency of non-linear amplifiers to linearly amplify any kind of constellation. These amplifiers are not perfects and symmetric, so they contribute to some phase and gains error in the transmitter, which can compromise the system performance. Phase imbalances can occur when some signals have different delay values at the combiner input. Under these conditions, the symbols associated to each branch suffer different rotations

which cause distortion of the resulting constellations after the combiner. Gain unbalances also compromise the system performance, with higher impact in the high order constellations [27].

This chapter presents a mathematical study and a set of performance results concerning the impact of non-matching power amplifiers for different phases and gains. Starting with a transmitter imbalance acting alone for a MSK constellation and then later on the transmitter described in the last section with constellation decomposition. Analysing the performance results would be possible to determine the amplifiers accuracy for a real system.

Impact on System Performance due to Inter-Symbol Interference (ISI)

Let us start by analysing the phase unbalance effects for a MSK constellation. To analyse the phase unbalance consequence in the system performance we will assume the receiver structure depicted in the Fig.3.6. As shown in the receiver structure, x(t) is the transmitted signal in the serial format, given by (3.19). The signal y(t) denotes the signal after the match filter at the receiver, and is computed by

$$y(t) = \sum_{n=0}^{N-1} a_n p(t - nT) + N_k, \tag{3.21}$$

where

$$p(t) = r(t) \otimes r^*(-t). \tag{3.22}$$

with the operator $\otimes$ denoting the convolution.

Denote that r(t) has 2T period, so the $p(t)$ signal has double length 4T. Thanks to it, the received signal seems to have ISI in the sampling periods kT. An example of $|y(t)|$ signal is represented in the Fig.3.7 by the solid lines. As can be denoted at the sampling periods kT, the $|y(t)|$ seems to have ISI. In the same figure is depicted the real component of the $|y(t)|$ (dashed lines), this component for $t = kT$ with $k \neq 0$ is equal to zero.

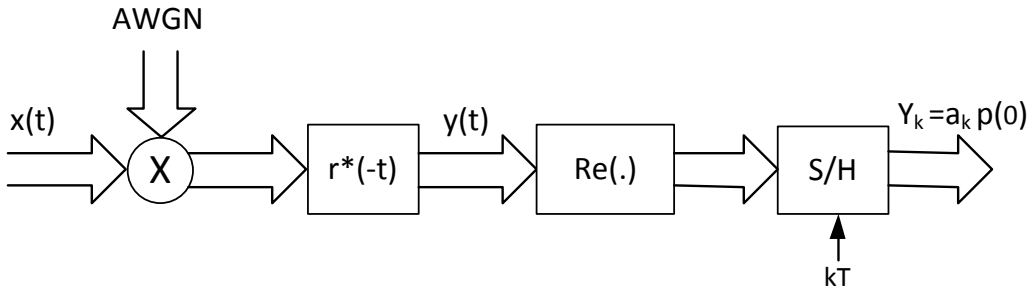

Figure 3.6: MSK receiver based on the serial stream

Therefore in the sampling periods kT we have

$$y(kT) = \sum_{n=0}^{N-1} a_n p(t-nT)\Big|_{t=kT} = \begin{cases} \alpha & for \quad k=0 \\ \pm j\beta & for \quad |k|=1 \\ 0 & for \quad |k|>1. \end{cases} \tag{3.23}$$

with β representing a complex component from the a_{k-1} and a_{k+1} in the a_k sampling time. Thence for a perfect balanced amplifiers the a_{k-1} and a_{k+1} pulses are not interfering in the a_k sampling, since they have real component null. In the other words, if $\theta = 0$ we don't have ISI.

Now we will consider a unbalanced transmitter phase, which is expected to decrease the system performance. We can write the transmitted signal as

$$x(t) \rightarrow x(t)\exp(j\theta) = \sum_{n=0}^{N-1} a_n r(t-nT)\exp(j\theta), \tag{3.24}$$

consequently the sampled signal y_k is given by

$$y_k = y(kT) = \Re\left\{\sum_{n=0}^{N-1} a_n p(t-nT)\exp(j\theta)\Big|_{t=kT}\right\}. \tag{3.25}$$

Taking into account the example in Fig.3.7 the y_k samples come as

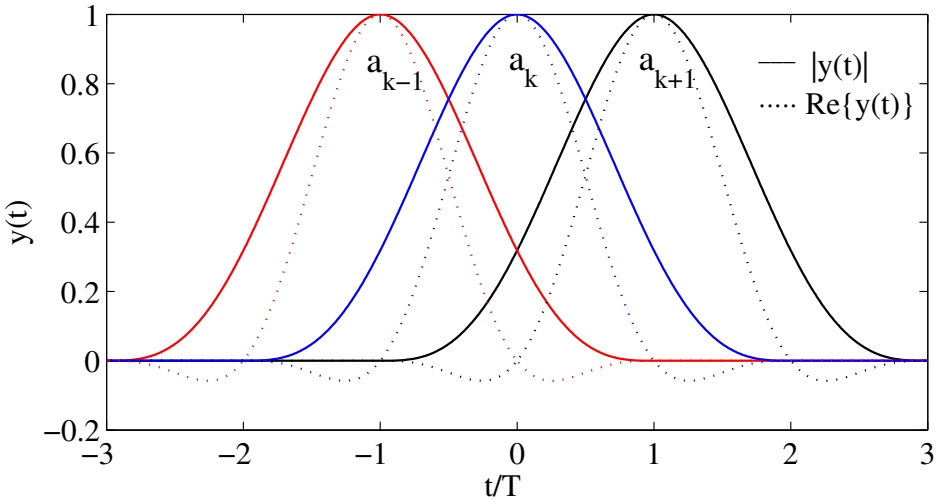

Figure 3.7: Received MSK signal after match filter

$$y_k = \Re\left\{a_k p(0)\exp(j\theta) + a_{k+1}p(-T)\exp(j\theta) + a_{k-1}p(T)\exp(j\theta)\right\} \tag{3.26}$$

$$= a_k\alpha\cos(\theta) + a_{k+1}\beta\sin(\theta) - a_{k-1}\beta\sin(\theta)$$

$$= a_k\alpha\left(cos(\theta) + \frac{a_{k+1}-a_{k-1}}{a_k}\frac{\beta}{\alpha}\sin(\theta)\right). \tag{3.27}$$

With phase unbalance the neighbour pulses are shifted, i.e. in the sampling time they don't have real component equal to zero, so they add with the actual pulse and cause undesirable distortion, which result in increasing at received Bit Error Rate (BER). Considering that a_k can take the values +1 or -1, the (3.27) can take the following values with the respectively probabilities

$$\begin{cases} \cos(\theta) & Prob.\frac{1}{2} \\ \cos(\theta) + \frac{\beta}{\alpha}\sin(\theta) & Prob.\frac{1}{4} \\ \cos(\theta) - \frac{\beta}{\alpha}\sin(\theta) & Prob.\frac{1}{4} \end{cases} \tag{3.28}$$

The BER expression for $\theta = 0$ is approximated by

$$Pb \approx Q\left(\sqrt{\frac{2E_b}{N_o}}\right). \tag{3.29}$$

A mathematical description of the BER for a signal in the presence of phase imbalances

introduced by the transmitter amplifiers is

$$\begin{aligned} Pb \approx & \frac{1}{2}Q\left(\sqrt{\frac{2E_b}{N_o}}\cos(\theta)\right) \\ & + \frac{1}{4}Q\left(\sqrt{\frac{2E_b}{N_o}}\left(\cos(\theta)+\frac{\beta}{\alpha}\sin(\theta)\right)\right) \\ & + \frac{1}{4}Q\left(\sqrt{\frac{2E_b}{N_o}}\left(\cos(\theta)-\frac{\beta}{\alpha}\sin(\theta)\right)\right) \end{aligned} \tag{3.30}$$

To evaluate the impact of the unbalanced phases in the power performance, is depicted in Fig.3.8 the BER for four different values of θ. It can be seen how performance decreases with the unbalance phase in the transmitter amplifiers.

Denote that we are not analysing the gain unbalance for this MSK example, since the gain is just affecting the pulse amplitude and is not producing ISI. This performance reduc-

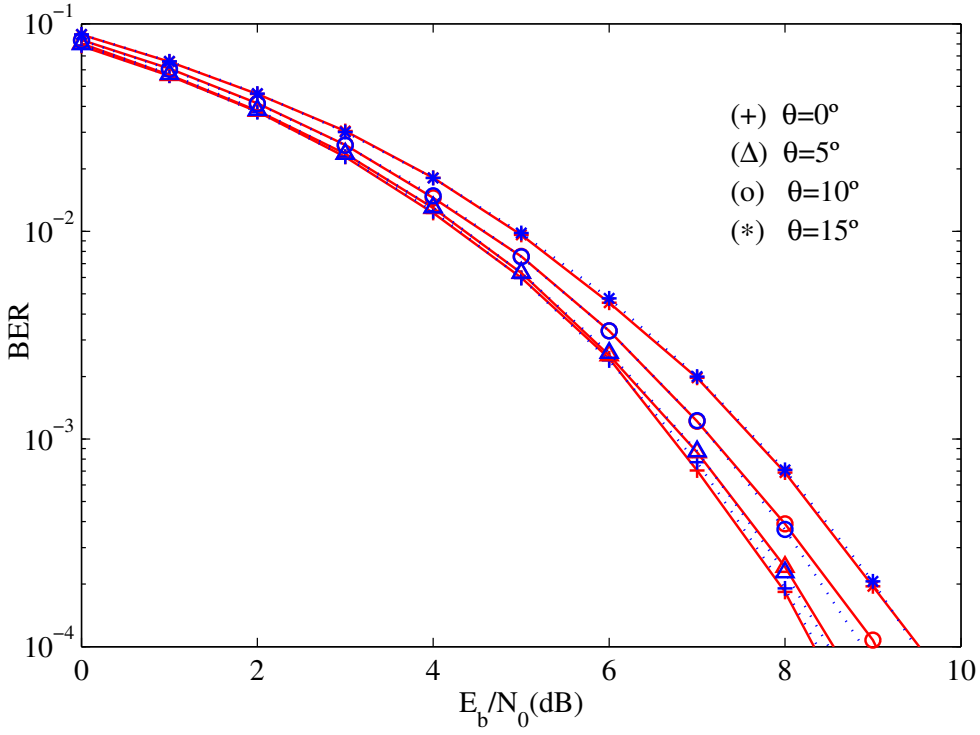

Figure 3.8: Simulated and mathematical BER performance for MSK

tion grows when we are taking into account the transmitter from the section 3.3, since we are representing the constellations as sum of BPSK and the gain and phase imbalances affects the constellation shape, as we will see in the next section.

Impact on Constellation Shape due to Non-Uniform Phase and Gain Imbalances

Considering a transmitter system as shown in the Fig.3.9 [28] where $s(t) = [s_I(t), s_Q(t)]^T$

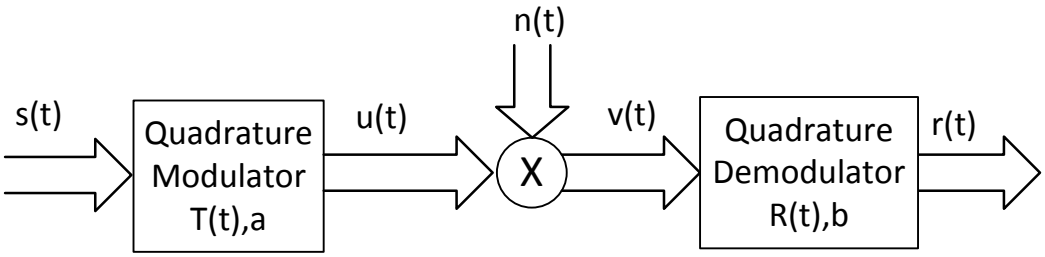

Figure 3.9: Example of transmitter system

presents the QAM output and the superscript T denotes the transpose operation. The quadrature modulator imperfections are modelled by a vector $a = [a_I, a_Q]^T$ and a 1×2 matrix $T(t)$ given by

$$T(t) = 2\left[k\cos(wt), \sin(wt + \phi)\right], \tag{3.31}$$

where w denotes the angular frequency, k is the gain imbalance and ϕ is the phase imbalance where magnitude is smaller than $\frac{\pi}{2}$. At the output of quadrature modulator we have the signal

$$u(t) = T(t)\left[s(t) + a\right]. \tag{3.32}$$

The quadrature demodulator is characterized by a vector $b = [b_I, b_Q]^T$ and the 1×2 matrix

$$R(t) = \left[l\cos(wt + \alpha), \sin(wt + \alpha + \gamma)\right]^T, \tag{3.33}$$

where α presents a constant phase difference between the transmitter oscillator and the receiver oscillator, l is the gain imbalance and γ the phase imbalance. The term $n(t)$ denotes the Additive White Gaussian Noise (AWGN) with simple side PSD of No. The

output signal is

$$r(t) = Hs(t) + Ha + b + n_r(t), \tag{3.34}$$

where H is the channel matrix and $n_r(t)$ denotes the noise after the Low-Pass Filter (LPF)

$$H = LPF\{R(t)T(t)\} \tag{3.35}$$

$$= LPF\{2\left[l\cos(wt+\alpha), \sin(wt+\alpha+\gamma)\right]^T \left[k\cos(wt), \sin(wt+\phi)\right]\} \tag{3.36}$$

$$= LPF\left\{2\begin{bmatrix} kl\cos(wt+\alpha)\cos(wt) & l\cos(wt+\alpha)\sin(wt+\phi) \\ k\sin(wt+\alpha+\gamma)\cos(wt) & \sin(wt+\alpha+\gamma)\sin(wt+\phi) \end{bmatrix}\right\} \tag{3.37}$$

$$= \begin{bmatrix} kl\cos(\alpha) & l\sin(\phi-\alpha) \\ k\sin(\alpha+\gamma) & \cos(\alpha+\gamma-\phi) \end{bmatrix}. \tag{3.38}$$

After LPF the noise is still Gaussian with the covariance matrix

$$c_{n_r,n_r} = \frac{NoB}{4}\begin{bmatrix} l^2 & l\sin(\gamma) \\ l\sin(\gamma) & 1 \end{bmatrix}. \tag{3.39}$$

where B represents the signal bandwidth.

If we assume ideal synchronization at the receiver, the receiver signal samples are

$$r(u) = Hs(u) + C + n_r(u), \tag{3.40}$$

the error vector is the difference between the transmitted and the received signal vectors namely

$$e(u) = r(u)s(u) = (H-I)s(u) + C + n_r(u) = e_r(u) + e_n(u). \tag{3.41}$$

$$\sigma_e^2 = E\left[e(u)^H e(u)\right] = E\left[e(u)^T e(u)\right] \tag{3.42}$$

$$= E\left[\left(s(u)(H-I) + C + n_r(u)\right)^T \left(s(u)(H-I) + C + n_r(u)\right)\right] \tag{3.43}$$

$$= E\left[s^T(u)(H-I)(H-I)s(u)\right] + E\left[C^T C\right] + E\left[n_r^T(u)n_r(u)\right] \tag{3.44}$$

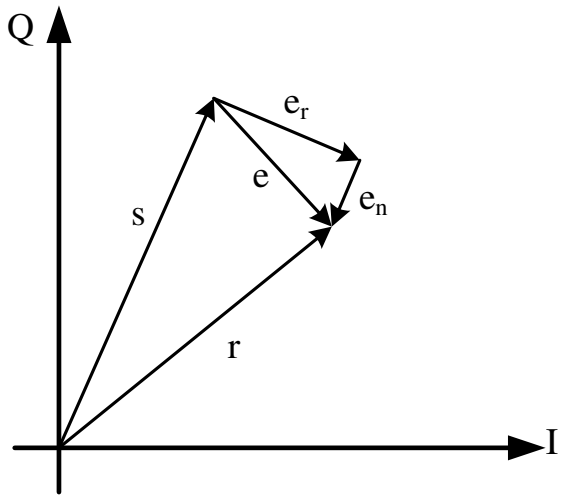

Figure 3.10: I-Q error graph

With $E\left[C^T C\right] = C^T C$

$$C^T C = \begin{bmatrix} l^2 & l\sin(\gamma) \\ l\sin(\gamma) & 1 \end{bmatrix} \begin{bmatrix} l^2 & l\sin(\gamma) \\ l\sin(\gamma) & 1 \end{bmatrix} \tag{3.45}$$

$$= l^4 + l^2\sin^2(\gamma), \tag{3.46}$$

$$and \tag{3.47}$$

$$Tr\left\{ \begin{bmatrix} kl\cos(\alpha) & k\sin(\alpha+\gamma) \\ l\sin(\phi-\alpha) & \cos(\alpha+\gamma-\phi) \end{bmatrix} \begin{bmatrix} kl\cos(\alpha) & l\sin(\phi-\alpha) \\ k\sin(\alpha+\gamma) & \cos(\alpha+\gamma-\phi) \end{bmatrix} \right\} \tag{3.48}$$

$$= (kl)^2\cos^2(\alpha) + k^2\sin^2(\alpha+\gamma) + l^2\sin^2(\phi-\alpha) + \cos^2(\alpha+\gamma-\phi) \tag{3.49}$$

where Tr represents the minimum of diagonal elements [29]. Phase imbalances in the transmitter can be decomposed to a deterministic part and a random part as

$$\phi = \phi_d + \phi_r \qquad with \qquad \phi_r \backsimeq N(0, \phi_{rms}^2), \tag{3.50}$$

assuming $\phi_{rms} \ll 1$, $l = 1$ and $\gamma = 0$ results from (3.47)

$$H = \begin{bmatrix} k\cos(\alpha) & \sin(\phi_d + \phi_r - \alpha) \\ k\sin(\alpha) & \cos(\alpha - \phi_d - \phi_r) \end{bmatrix} \tag{3.51}$$

$$= \begin{bmatrix} k\cos(\alpha) & \sin(\phi_d - \alpha) \\ k\sin(\alpha) & \cos(\alpha - \phi_d) \end{bmatrix} + \phi_r \begin{bmatrix} 0 & \cos(\phi_d - \alpha) \\ 0 & \sin(\alpha - \phi_d) \end{bmatrix} \tag{3.52}$$

$$= H_d + \phi_r H_0 \tag{3.53}$$

if $\alpha = 0$,i.e, a null phase difference between the transmitter and receiver, then

$$H = \begin{bmatrix} k & \sin(\phi_d) \\ k & \cos(-\phi_d) \end{bmatrix} + \phi_r \begin{bmatrix} 0 & \cos(\phi_d) \\ 0 & \sin(-\phi_d) \end{bmatrix} \tag{3.54}$$

3.5 Symbol Error Rate Calculation

For Symbol Error Rate (SER) calculation we consider a M-QAM constellation with all possible symbols belonging to an alphabet S. The corresponding modulated vectors are defined as a vector alphabet $V = V_1, V_2, V_3, ..., V_N$. Therefore for a given transmitted signal vector $S(u) \in V$ the received vector is

$$r(u) = S(u) + e_S(u) + e_n(u), \tag{3.55}$$

where $S(u) + e_S(u)$ is a deterministic component and $e_n(u)$ represents a random component. From the covariance matrix results for the Gaussian noise the joint normal Probability Density Function (PDF)

$$F_{e_n}(X, Y) = A \exp\left\{ -\frac{2}{N_o B(1 - \sin^2(\gamma)} \left[\frac{X^2}{l^2} - 2\sin(\gamma)\frac{XY}{l} + Y^2 \right] \right\} \tag{3.56}$$

with $A = \dfrac{2}{\pi N_o B l \sqrt{1 - \sin^2(\gamma)}}$ where X and Y denotes the I and Q components of the received noise vector that are zero mean random variables with variance and correlation given by the covariance matrix above. Since noise term is independent of the signal, the

received noise component have identical PDF and are not related with different transmitted signal vectors.

Therefore, for the receiver vector results the conditional PDF given by

$$F_{r(u)|s(u)}(X,Y) = F_{e_n}\left(X - \overline{r_x}(u), Y - \overline{r_y}(u)\right)$$
$$= A\exp\left\{-\frac{4}{N_o B(1-\sin^2(\gamma)}\left[\frac{(X-\overline{r_x}(u))^2}{l^2} - 2\sin(\gamma)\frac{(X-\overline{r_x}(u))(Y-\overline{r_y}(u))}{l} + (Y-\overline{r_y}(u))^2\right]\right\} \tag{3.57}$$

with $\overline{r_x}(u)$ and $\overline{r_y}(u)$ the I and Q components of the deterministic part of the received vector. Therefore $\overline{r_x}(u)$ and $\overline{r_y}(u)$ are the mean values of the I and Q components of the receiver array.

We assume that QAM modulated vectors are demodulated using a hard decision criterion. Consequently the demodulation of the QAM symbols is done by choosing the symbol that minimizes the euclidean distance between the received signal and a signal in the vector alphabet.

For a decision region D_i the conditional detection probability is given by

$$P_{D_i} = \iint\limits_{D_i} F_{r(u)|s(u)} = (E-Z)_i(X,Y)dxdy \tag{3.58}$$

The conditional error probability is given by

$$P_{e_i} = 1 - P_{d_i} \tag{3.59}$$

For edge points and corner points of the constellation the decision can be expressed as

$$D_i = \{X, Y | X \in (a_i, b_i) Y \in (c_i, d_i)\} \tag{3.60}$$

where the boundaries can be finite or infinite.

Therefore results for detection probability

$$P_{D_i} = \int_{ci}^{di}\int_{ai}^{bi} A\exp\left\{-\frac{4}{N_o B(1-\sin^2(\gamma)}\left[\frac{(X-\overline{r_x}(u))^2}{l^2} - 2\sin(\gamma)\frac{(X-\overline{r_x}(u))(Y-\overline{r_y}(u))}{l}\right.\right.$$
$$\left.\left. + (Y-\overline{r_y}(u))^2\right]\right\}dxdy. \tag{3.61}$$

Assuming that all symbols in the constellation have the same probability to be sent, the total SER is the average of the conditional detection error probability of each symbol as

$$P_e = \frac{1}{N}\sum_{i=0}^{N-1} P_{e_i} \tag{3.62}$$

which represents the analytical expression of the SER for an M-QAM system in the transceiver imbalances and channel noise.

3.6 Performance results over AWGN channel

Let us present a set of performance results regarding the use of Single-Carrier with Frequency-Domain Equalization (SC-FDE) modulation with FFT-block of N=256 data symbols and cycle prefix of 32 symbols, longer than overall delay spread of the channel. We consider a AWGN channel and perfect channel estimation at the receiver. All performance results are expressed as function of $\Delta(Phase/Gain)$ and $\sigma(Phase/Gain)$, where $\Delta(Phase/Gain)$ denotes the fixed value of Phase and Gains imbalances between the transmitter and the receptor and $\sigma(Phase/Gain)$ represents a value from Gaussian distribution with variance σ of Phase and Gain imbalances, leading to imbalances in the transmitter amplifiers. The $\Delta(Phase/Gain)$ imbalances affect all constellation by a regular offset, leading to a output constellation with the symbols diverted from the original decision bounds. The receiver used can not recover from this because the decision bounds are fixed. The $\sigma(Phase/Gain)$ imbalances induce non uniform offset in the parallel amplification stage, producing a non regular constellations shape. Due to the Gaussian distribution each BPSK component is subjected to the different offset, so the resultant constellation symbols will change the position to a random new one.

Figures 3.11, 3.12, 3.13 and 3.14 show the imbalances impact at system performance for a

16, 32 and 64 QAM and Voronoi constellation for $E_b/N_0 = 12, 14, 16$ respectively. Clearly constellations with higher number of symbols have more sensitivity to phase and gain imbalances, since the decision boundaries are more limited and accurate. Voronoi constellation exhibit worst performance when compared with the same size QAM. Due the energy optimization where the symbols are diffused to create a minimum energy constellation, Voronoi constellations suffer more from gain and phase imbalances, since the symbols configurations are densest.

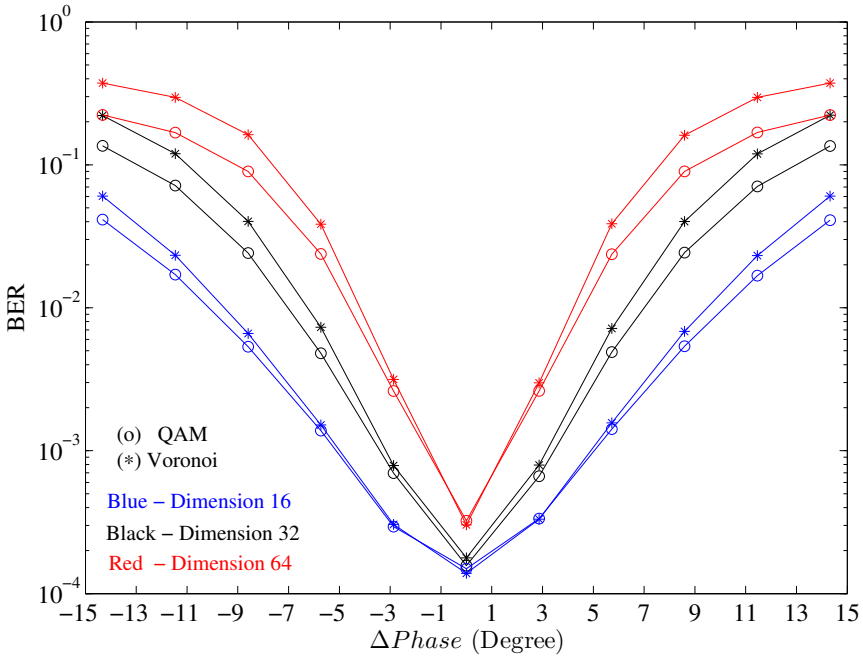

Figure 3.11: BER performance results for M-QAM and Voronoi in AWGN channel with $E_b = 12, 14, 16$ for ΔPhase imbalances

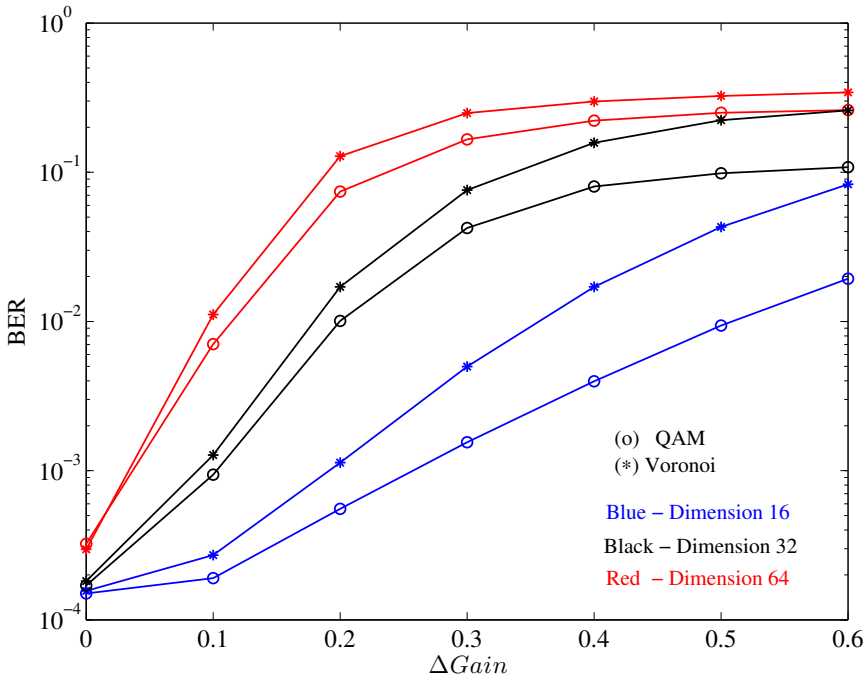

Figure 3.12: BER performance results for M-QAM and Voronoi in AWGN channel with $E_b = 12, 14, 16$ for ΔGain imbalances

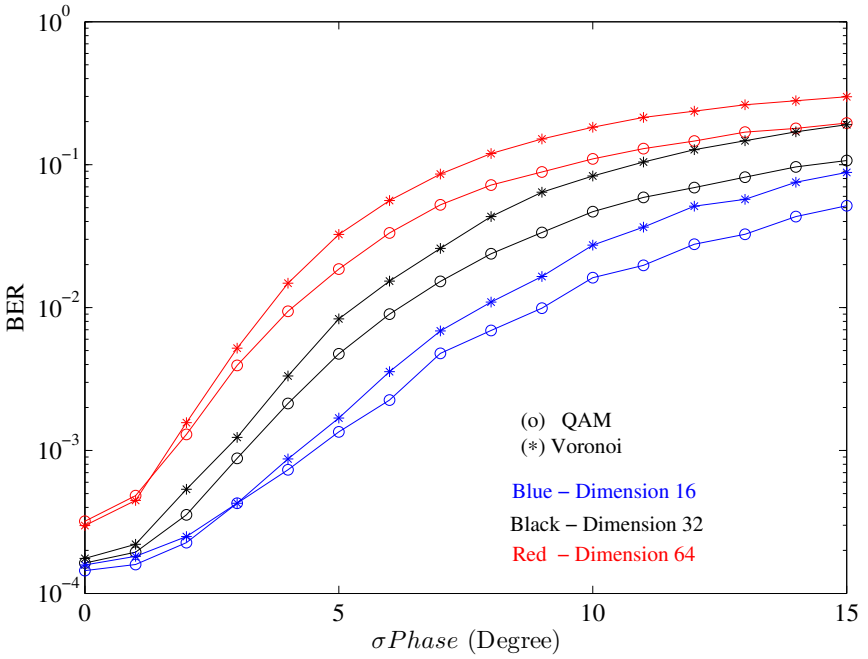

Figure 3.13: BER performance results for M-QAM and Voronoi in AWGN channel with $E_b = 12, 14, 16$ for σPhase imbalances

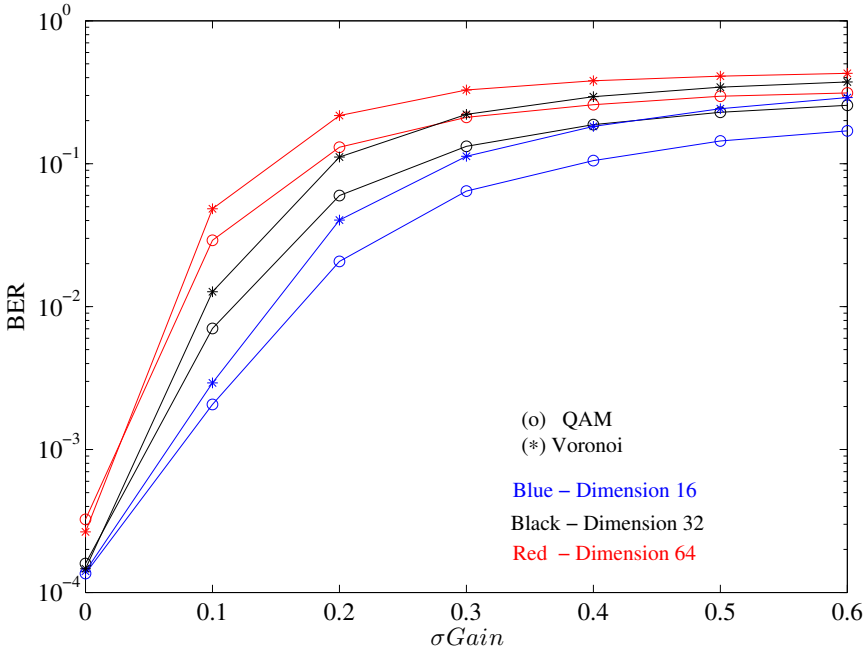

Figure 3.14: BER performance results for M-QAM and Voronoi in AWGN channel with $E_b = 12, 14, 16$ for σGain imbalances

4

Receiver Design SC-FDE

Alike the earthly wireless communication with high bit rates, in satellite communications, the data is affected by the time-dispersion effects due to the multi-path propagation. To overcome these effects, equalization techniques at the receiver side become necessary to compensate the signal distortion and ensure good performance.

The time-domain equalizers have been applied to digital communications systems to compensate the Inter-Symbol Interference (ISI) at the receiver, however for the severely time-dispersive channels the complexity and digital processing speed become impractical [30]. Some transmission schemes, using blocks with Cyclic Prefix (CP) and employing a Frequency-Domain Equalization (FDE), proved to be appropriate to transmit with high data rates over severely dispersive channels without requiring complex receiver implementation.

Multi-Carrier (MC) modulation emerge as a solution to deal with the effects of dispersive channels as alternative to Single-carrier (SC). Orthogonal Frequency Division Multiplexing (OFDM) has become popular and widely used in many wireless systems operating in the frequency-selective fading radio channel. OFDM employs frequency domain equalization, performed on a data block, which is less complex to implement than time domain equalization. Using a Inverse Discrete Fourier Transform (IDFT) in the transmitter to generate the multiple sub-carriers OFDM, the extraction of sub-carriers at receiver is done by

the inverse function Discrete Fourier Transform (DFT).

A good alternative to OFDM is to use Single-Carrier with Frequency-Domain Equalization (SC-FDE), where non-linear equalizer receivers are implemented in the frequency domain employing Fast Fourier Transform (FFT), which gives the same performance and low complexity as OFDM[5].

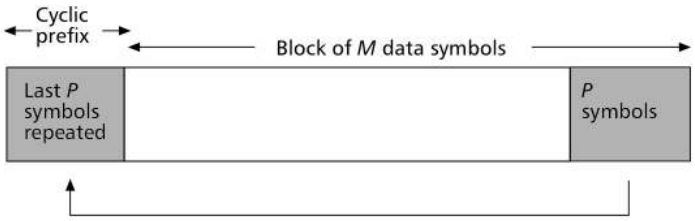

Figure 4.1: Cyclic prefix illustration

The block transmission schemes including a CP have shown to be very efficient. The CP is a repetition of last data symbol included in the beginning of each block, as shown in Fig.4.1.The CP must be longer than Channel Impulse Response (CIR), but short enough to maintain the spectral efficiency. Therefore the CP prevent the ISI for OFDM and SC-FDE schemes over multi-path channels and make the received blocks appear to be periodic. This allow the circular convolution use, which is essential for DFT and operation.

Due to the large Peak-to-Average Power Ratio (PAPR), a OFDM transmitter require a linear amplifier with some power backed off several dB's, this fact leads to a significant low power efficiency. The low PAPR of SC-FDE allows an efficient power amplification with non-linear amplifiers. [4].

4.1 Linear FDE

The performance of SC-FDE systems is similar to that of OFDM, even for very long channel delay spread and is inherently more efficient in terms of power consumption, due to the reduced PAPR. However, there is one significant difference between both systems, the decision about the transmitted bits: in OFDM this decision is done in the frequency

domain while in the SC-FDE the same decision is performed in the time domain. This difference affects the IDFT block position in each system. The OFDM has the IDFT block placed in transmitter while SC-FDE has the same block in the receiver as we can see in Fig.4.3 and Fig.4.2

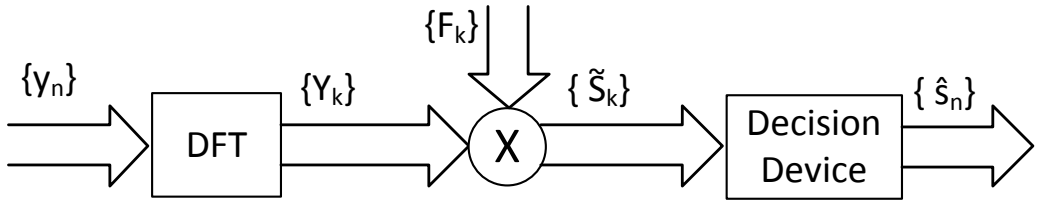

Figure 4.2: OFDM receiver structure

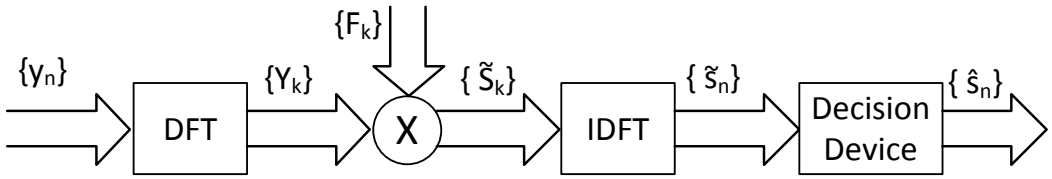

Figure 4.3: SC-FDE receiver structure

A SC-FDE structure is depicted in Fig.4.3 where $\{y_n; n = 0, 1, ..., N-1\}$ are the received time-domain samples. From these samples after N-point DFT results the corresponding frequency-domain block $\{Y_k; nk = 0, 1, ..., N-1\}$ with Y_k given by

$$Y_k = H_k S_k + N_k, \qquad k = 0, 1, ..., N-1 \tag{4.1}$$

where H_k and N_k, denotes the overall channel frequency response and channel noise term in the frequency-domain for the k^{th} frequency of the block respectively. To cope with the dispersive channel effects a linear FDE can be employed. For a given block, the

output samples $\tilde{S_k}$ for each k^{th} sub-carrier are given by

$$\tilde{S_k} = F_k Y_k \tag{4.2}$$

where the set of coefficients $\{F_k; k = 0, 1, ..., N-1\}$ denotes the feedforward FDE coefficients. For a Zero-Forcing (ZF) equalizer the coefficients F_k are given by

$$F_k = \frac{1}{H_k} = \frac{H_k^*}{|H_k|^2}, \tag{4.3}$$

For frequency selective channels the drawback of ZF criterion is the noise enhancement at sub-channels with deep notches.The Minimum Mean Square Error (MMSE) criterion to minimize both effects of ISI and channel noise enhancement where F_k coefficients can be given by

$$F_k = \frac{H_k^*}{\beta + |H_k|^2}, \tag{4.4}$$

where β denotes the inverse of the Signal-to-Noise Ratio (SNR), given by

$$\beta = \frac{\sigma_N^2}{\sigma_S^2} \tag{4.5}$$

where $\sigma_N^2 = \frac{E[|N_k|^2]}{2}$ and $\sigma_S^2 = \frac{E[|S_k|^2]}{2}$ denotes the variance of the real and imaginary parts of the channel noise components $\{N_k; k = 0, 1, ..., N-1\}$ and the data samples $\{S_k; k = 0, 1, ..., N-1\}$, respectively. β is a noise-dependent term which avoids noise enhancement effects when the channel has very low values of the frequency response. The IDFT block converts back the equalized samples $\{\tilde{S_k}; k = 0, 1, ..., N-1\}$ to the time-domain $\{\tilde{s_n}; n = 0, 1, ..., N-1\}$. These samples now can be submitted to the decision block to make the decisions on the transmitted bits.

4.2 Iterative Block Decision Feedback Equalization (IB-DFE)

The linear equalization, in the frequency domain, is better than a equalization in the time-domain. However the performance results are distant from the Matched Filter Bound (MFB) performance, as we can see from Fig.4.4.

It is well-know that Decision Feedback Equalization (DFE), as proposed in [5], have better performance than linear ones. For this reason a hybrid time-frequency-domain with the time-domain feedforward filter and feedback frequency-domain filter was propose in [31]. This hybrid DFE approach can suffer from error propagation when the feedback filters have a large number of taps.

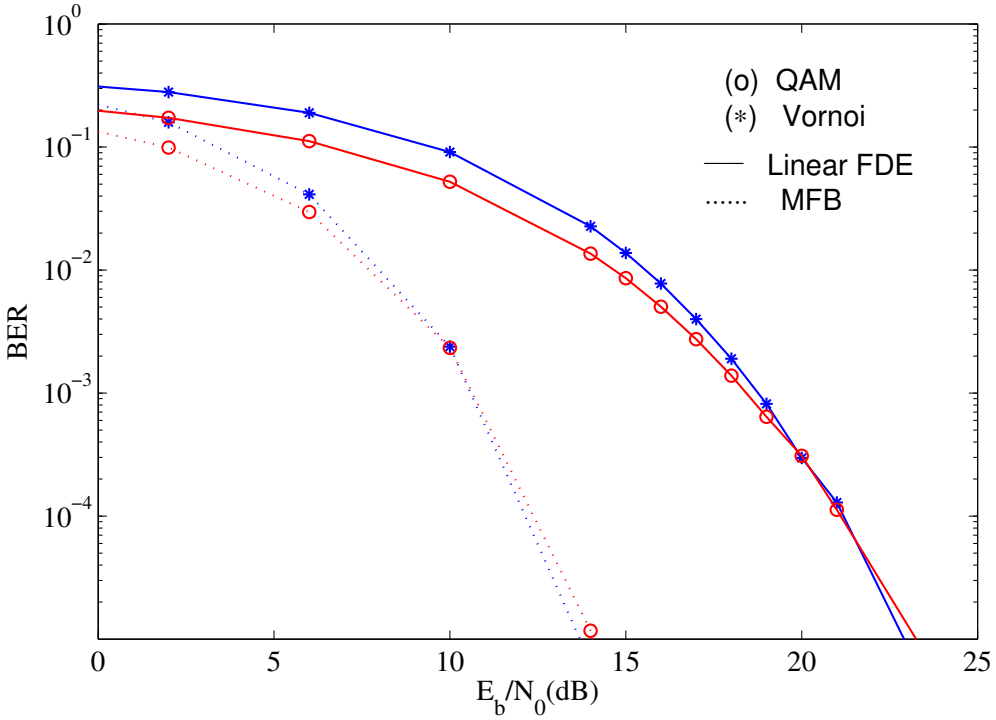

Figure 4.4: SC-FDE linear performance with 16-QAM and 16-Voronoi constellations

A promising IB-DFE was proposed for a performance improvement in [6]. A IB-DFE is an iterative DFE for SC-FDE where feedback and feedforward filters are implemented in the frequency-domain as shown in Fig.4.5 For a given iteration i the frequency-domain samples at the output of the IB-DFE are given by

$$\tilde{S_k}^{(i)} = F_k^{(i)} Y_k - B_k^{(i)} \hat{S_k}^{(i-1)}, \tag{4.6}$$

where $\{F_k^{(i)}; k = 0, 1, ...N-1\}$ and $\{B_k^{(i)}; k = 0, 1, ...N-1\}$ denote the feedforward and feedback coefficients, respectively and $\{\hat{S_k}^{(i-1)}; k = 0, 1, ...N-1\}$ denotes a DFT of the estimated block $\{\hat{s_n}^{(i-1)}; n = 0, 1, ...N-1\}$, with $\hat{s_n}^{(i-1)}$ denoting the hard-estimate of s_n

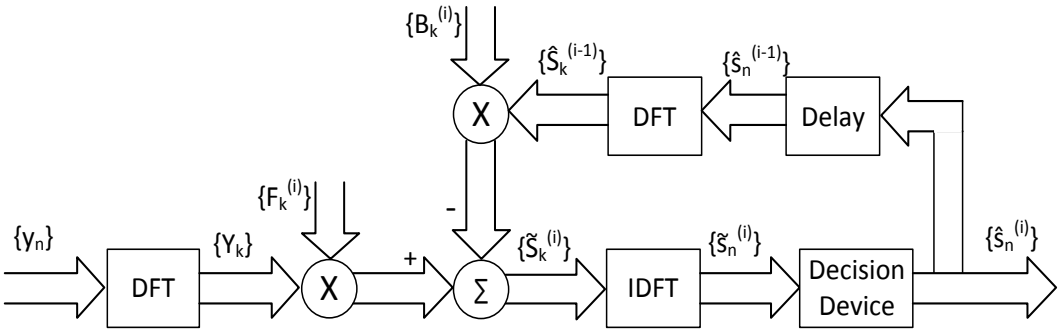

Figure 4.5: IB-DFE with "hard-decisions" receiver structure

from the previous DFE iteration.

The feedforward and feedback IB-DFE coefficients $F_k^{(i)}$ and $B_k^{(i)}$, are chosen in order to maximize the Signal-to-Interference plus Noise Ratio (SINR). Considering an IB-DFE hard decisions with the optimum feedforward coefficients are given by [7]

$$F_k^{(i)} = \frac{\kappa H_k^*}{\beta + \left(1 - \left(\rho^{(i-1)}\right)^2\right)|H_k|^2}, \tag{4.7}$$

with the feedback coefficients calculated by

$$B_k^{(i)} = \rho^{(i-1)}\left(F_k^{(i)} H_k - 1\right), \tag{4.8}$$

where κ is selected to ensure that

$$\sum_{k=0}^{N-1} F_k H_k / N = 1 \tag{4.9}$$

The β coefficient is given by (4.5) and the correlation coefficient from the previous iteration is defined as

$$\rho = \frac{E\left[\hat{S}_k S_k^*\right]}{E\left[|S_k|^2\right]} = \frac{E\left[\hat{s_n} s_n^*\right]}{E\left[|s_n|^2\right]}. \tag{4.10}$$

The correlation coefficient ρ, measures the reliability of the decisions and it is determinant to ensure a good receiver performance. In the way to reduce the error propagation problems the hard-decisions for each block and the overall block reliability are taking

into account in the feedback loop. For the first iteration there is no information about s_n, which means that $\rho = 0$, $B_k^{(0)}$ and $F_k^{(0)}$ coefficients are given by (4.4). Thereby, for the first iteration the IB-DFE acts as a linear FDE.

For the forward iterations, and if the residual Bit Error Rate (BER) is not too high, the feedback coefficients can be applied to reduce the residual interference. After several iterations, $\rho \backsimeq 1$ and the biggest part of residual ISI is cancelled. In Fig.4.6 it is shown the signal at the IB-DFE with "hard-decisions" $\hat{s_n}$ where is visible the interferences reduction with the number of iterations.

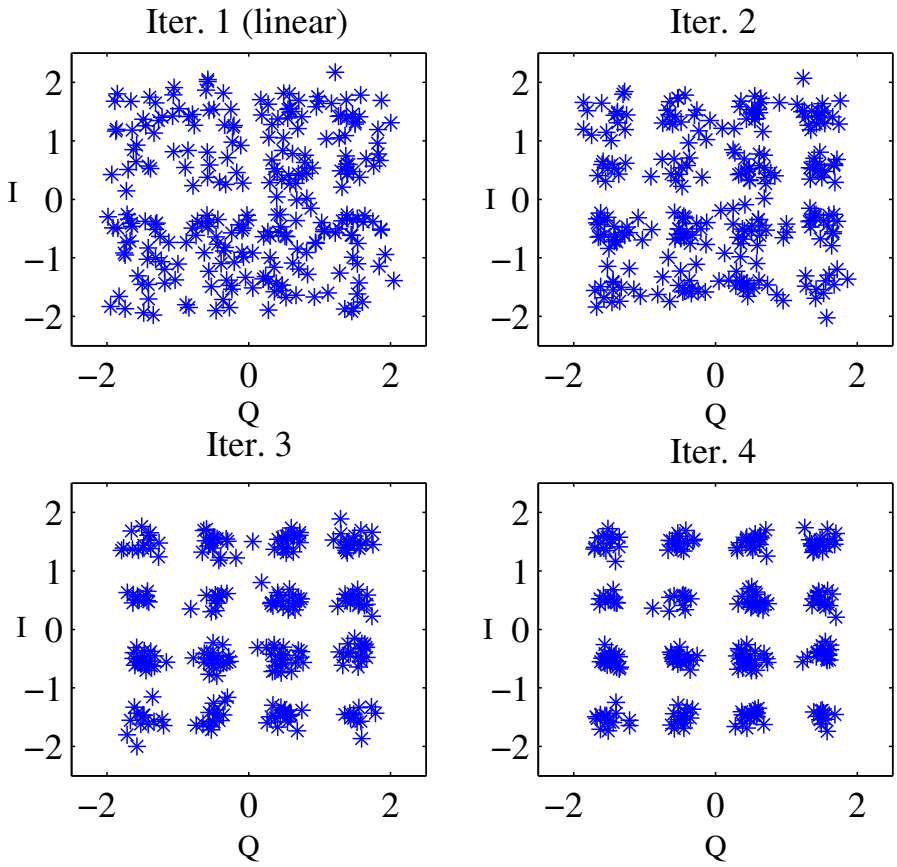

Figure 4.6: 16-QAM constellation signal at IB-DFE with "hard-decisions" output $\hat{s_n}$

IB-DFE with Soft Decisions

To improve the IB-DFE performance we can replace the "hard-decisions" $\{\hat{s_n}^{(i)}; n = 0, 1, ..., N-1\}$ by "soft-decisions" $\{\overline{s_n}^{(i)}; n = 0, 1, ..., N-1\}$. Therefore are used "symbols averages",

$\overline{s_n}^{(i)}$, instead of "blockwise averages". Now from (4.6) results

$$\tilde{S_k}^{(i)} = F_k^{(i)} Y_k - B_k^{(i)} \overline{S_k}^{(i-1)}, \tag{4.11}$$

with

$$\overline{S_k}^{(i-1)} = \rho^{(i-1)} \hat{S_k}^{(i-1)}. \tag{4.12}$$

Since $\rho^{(i-1)}$ is a measure of the blockwise reliability of the estimates $\hat{S_k}^{(i-1)}$, then $\overline{S_k}^{(i-1)}$ is the overall block average of $S_k{}^{(i-1)}$ at FDE output [10] [12]. The receiver structure for IB-DFE with "soft-decisions" is depicted in Fig.4.7. We may observe that feedforward coefficients used at both receivers are given by (4.7). At the FDE output, the time-domain samples $\tilde{s}_n^{(i)}$ are de-mapping into the corresponding bits. This is implemented by computing the log-likelihood ratios to each bit of the transmitted symbols [32]. The Log-

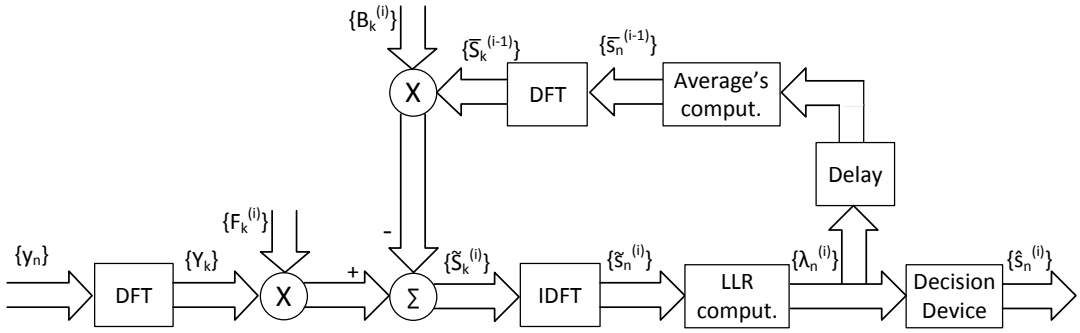

Figure 4.7: IB-DFE with "soft-decisions" receiver structure

Likelihood Ratio (LLR) of the mth bit from the nth transmitted symbol is given by

$$\begin{aligned} \lambda_n^{(m)} &= \log\left(\frac{Pr(\beta_n^{(m)}=1|\overline{s}_n)}{Pr(\beta_n^{(m)}=0|\overline{s}_n)}\right) \\ &= \log\left(\frac{\sum_{s\in\Psi_1^{(m)}} \exp\left(-\frac{|\tilde{s}_n - s|^2}{2\sigma^2}\right)}{\sum_{s\in\Psi_0^{(m)}} \exp\left(-\frac{|\tilde{s}_n - s|^2}{2\sigma^2}\right)}\right) \end{aligned} \tag{4.13}$$

where $\Psi_0^{(m)}$ and $\Psi_1^{(m)}$ are the subsets of $\mathfrak{G}$ where $\beta_n^{(m)}$ = 1 or 0 respectively, with $\mathfrak{G}$ representing all constellation symbols. Denote that $\Psi_0^{(m)} \cup \Psi_1^{(m)} = \mathfrak{G}$ and $\Psi_0^{(m)} \cup \Psi_1^{(m)} = \emptyset$, an

example of these subsets for a 8-Pulse Amplitude Modulation (PAM) constellation with Gray mapping is shown in Fig.4.8

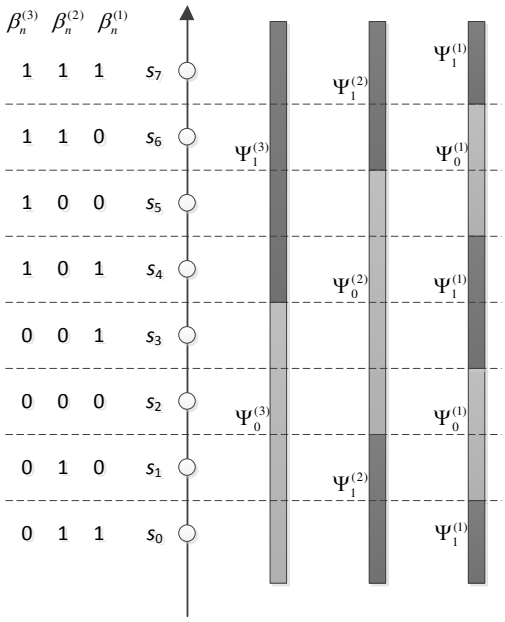

Figure 4.8: Regions associated to $\Psi_0^{(m)}$ and $\Psi_1^{(m)}$ (m=1,2,3) for a uniform 8-PAM constellation with Gray mapping

We can write the (4.13) in the following format

$$\lambda_n^{(m)} = \log\left(\sum_{s\in\Psi_1^{(m)}} \exp\left(-\frac{|\tilde{s}_n - s|^2}{2\sigma^2}\right)\right) - \log\left(\sum_{s\in\Psi_0^{(m)}} \exp\left(-\frac{|\tilde{s}_n - s|^2}{2\sigma^2}\right)\right), \tag{4.14}$$

To reduce the system complexity the following approximation can be taken into account

$$log(\exp(a) + \exp(b)) \approx log(\exp(\max(a,b))) = \max(a,b) = \min(-a,-b) \tag{4.15}$$

Assuming the (4.15) approximation and applying this result to the (4.14), the log-likelihood coefficients can be written as

$$\lambda_n^{(m)} = \min\left(\sum_{s\in\Psi_1^{(m)}} -d_{\tilde{s}_n,s}\right) - \min\left(\sum_{s\in\Psi_0^{(m)}} -d_{\tilde{s}_n,s}\right) \tag{4.16}$$

with

$$d_{\tilde{s}_n,s} = \frac{|\tilde{s}_n - s|^2}{2\sigma^2}. \tag{4.17}$$

This way of compute the log-likelihood coefficients is simpler and faster, which don't compromise the receiver performance and makes it less complex, when compared to the original way given by (4.13). The evolution of LLR coefficients of the different bits as function of FDE output $\tilde{s}_n$, for some SNR values, is depicted in Fig.4.9.

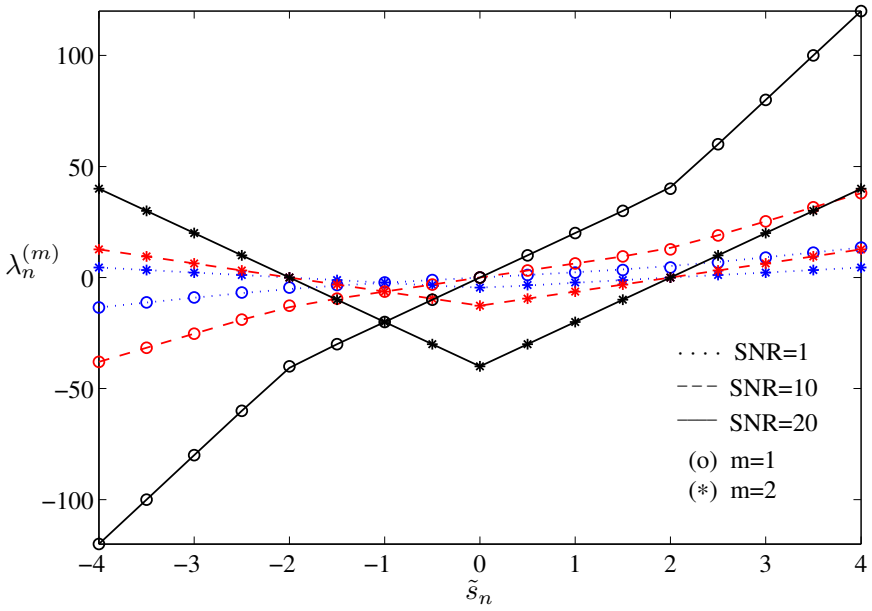

Figure 4.9: Log-likelihood coefficients evolution, computed with the accurate equation (4.13) and the approximated equation (4.16), represented with lines and marks respectively

Therefore to obtain the average symbols $\bar{b}_n$ at the FDE output, we must first compute the average bit values $\bar{b}_n^{(m)}$. These are related to the corresponding log-likelihood ratio as following equation

$$\bar{b}_n^{(m)} = \tanh\left(\frac{\lambda_n^{(m)}}{2}\right). \tag{4.18}$$

It should be noted that in Fig.4.10 the regions where each bit is 0 or 1 are clear for high SNR values, and are not so evident for low SNR.

We can take advantage of the analytical mapping rules defined in chapter 2 where the symbols constellations are expressed as function of the corresponding bits to compute

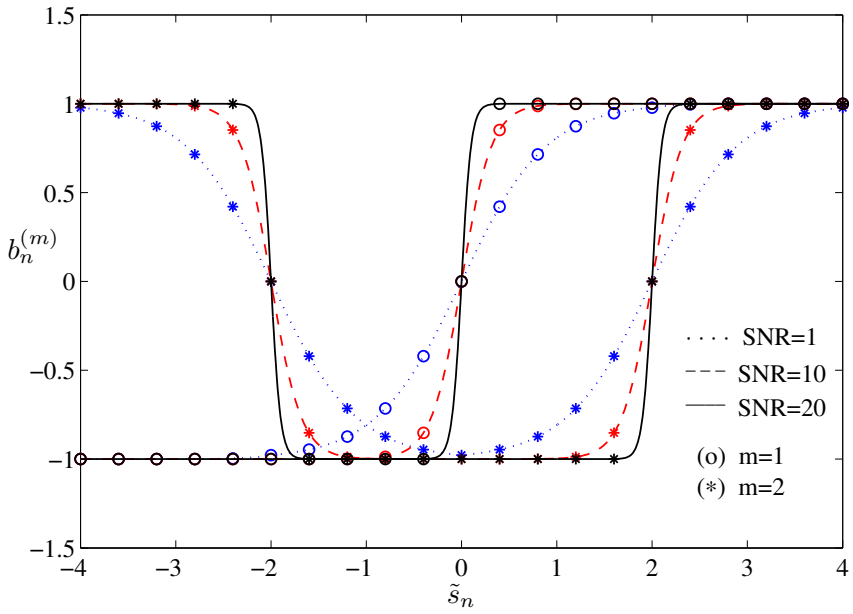

Figure 4.10: Average bit values $\overline{b}_n^{(m)}$ evolution, conditioned to the FDE output $\tilde{s}_n$, for each carrier of 16-QAM constellation with Gray mapping

the average symbols values for general constellations. Therefore, from (2.17) and (4.18) results

$$\overline{s}_n = \sum_{i=0}^{M-1} g_i \prod_{m=1}^{\mu} \left(\tanh\left(\frac{\lambda_n^{(m)}}{2} \right) \right)^{\gamma_{m,i}} \tag{4.19}$$

In Fig.4.11 it is shown the average symbol value $\overline{s}_n$ conditioned to the FDE output $\tilde{s}_n$, for some values of SNR. Similarly to the previous figures, for high SNR the 4 different decision regions are well defined. Unlike for low SNR values the transitions become smoother and the levels are not well delimited. Based on (4.19) and using the generic mapping rules of chapter 2, we can compute the reliability of estimates coefficient ρ for general constellations by

$$\rho = \frac{E\left[\hat{s_n} s_n^*\right]}{E\left[|s_n|^2\right]} = \frac{\sum_{i=0}^{M-1} |g_i|^2 \prod_{m=1}^{\mu} (\rho_n^m)^{\gamma_{m,i}}}{\sum_{i=0}^{M-1} |g_i|^2}, \tag{4.20}$$

where $\rho_n^{(m)}$ is the reliability of the mth bit of the nth transmitted symbol, given by

$$\rho_n^{(m)} = |b_n^{(m)}| \tag{4.21}$$

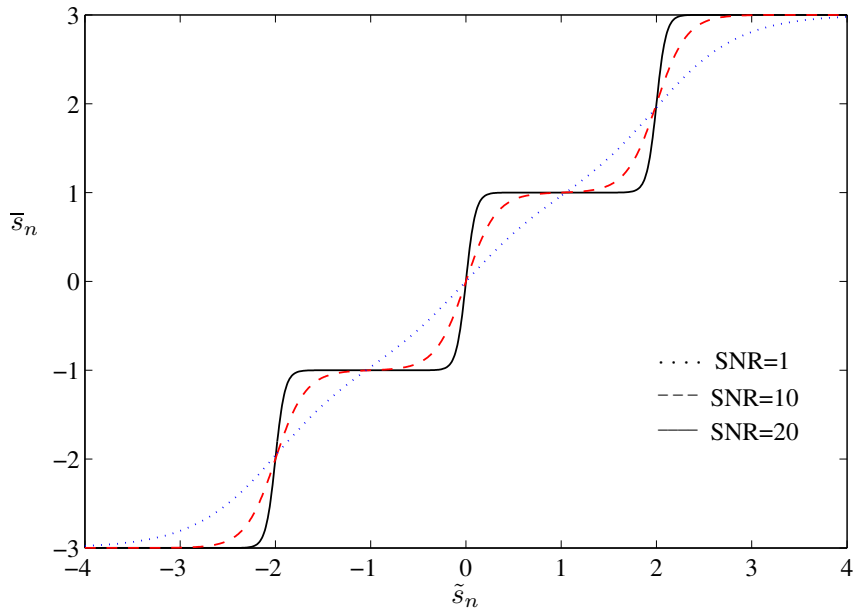

Figure 4.11: Average symbol values $\bar{s}_n^{(m)}$ evolution, conditioned to the FDE output $\tilde{s}_n$, for each carrier of 16-QAM constellation with Gray mapping

Let us now compare the performance of the IB-DFE receiver with "soft-decision" and

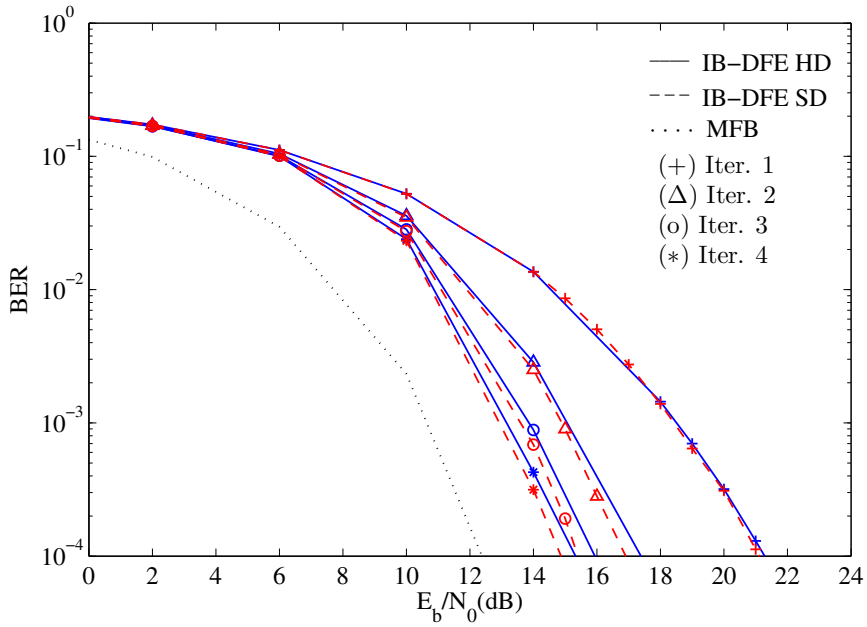

Figure 4.12: IB-DFE "hard-decisions" and "soft-decisions" performance with 16-QAM constellation

"hard-decisions". Figure 4.12 shows the 16-QAM constellation performance for both receivers, over a severely frequency fading channel. The performance improves with the

number of iteration on IB-DFE receiver, this improvement is more than 6dB for the "soft-decisions" and about 6db for "hard-decisions" receivers. Clearly the "soft-decisions" receiver outperforms the "hard-decisions" one, as was expected.

4.3 Performance Results

Here we present a set of performance results regarding the use of the proposed IB-DFE receiver in the time-varying channels. We consider a SC-FDE modulation, with FFT-block of N=256 data symbols and a cycle prefix of 32 symbols, longer than overall delay spread of the channel. The modulation symbols belong to a M-QAM or Voronoi constellation and are selected from the transmitter data according to a mapping rule that optimizes energy efficiency. We consider a severely time-dispersive channel characterized by a uniform Power Delay Profile (PDP), with 32 equal-power taps, with uncorrelated rayleigh fading on each tap. The degradation due to the useless power spent on the cycle prefix is not included.

Perfect Matching and Balance Performance

In this section is considered linear power amplification at the transmitter, perfect synchronization and channel estimation at the receiver. All performance results are expressed as function of E_b/N_0, where N_0 denotes the one-sided power spectral density of the noise and E_b is the energy of the transmitted bits.

Fig.4.13 shows the typical BER performance for both constellations types over an Additive White Gaussian Noise (AWGN) channel. As expected, Voronoi constellations have worst performance outside the asymptotic region due the higher number of neighbouring symbols. In the asymptotic region, Voronoi constellations lean to have similar or better performance than QAM constellations. For example, the 64 Voronoi constellation has a slight better performance than a equivalent QAM. The same conclusion is still valid, but less visible for the results depicted for the others constellation sizes. It should be noted that both cases have performances close to the MFB. Let us consider now the impact of severely frequency dispersive channel. Figures 4.14, 4.15 and 4.16 show the BER

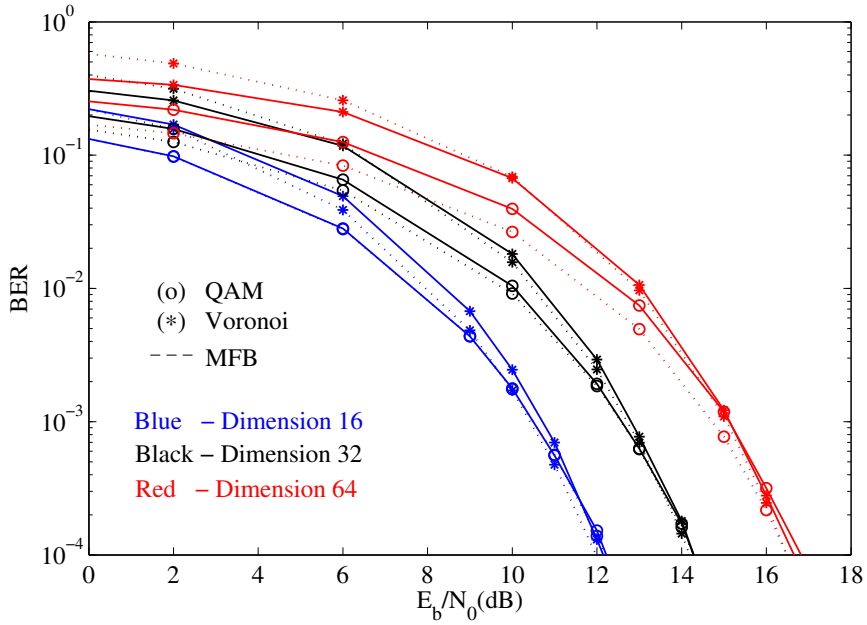

Figure 4.13: Performance results for M-QAM and Voronoi optimized constellations in AWGN channel

performance of both constellations, over severely frequency fading channel. Clearly the performance improves significantly with the number of iterations on IB-DFE, more for the first two iterations, because they reduce a major part of the residual interference. This improvement is higher for constellations with higher number of symbols, since they suffer more from the residual ISI that is inherent to a linear FDE optimized under MMSE criterion. As we can see from the results, despite the greater sensitivity to residual ISI of Voronoi constellations, when compared with M-QAM constellations, the performance of Voronoi constellations improves with the number of iterations, leading to similar or better performance results than the correspondent M-QAM constellations. For example for BER=10^{-4} the 64 symbols Voronoi constellations has slight better performance than the equivalent QAM. It should be mentioned that the same is not so visible for the others constellation sizes.

Clearly, any increase in the sensitivity to ISI due the energy optimization can be fully compensated with the IB-DFE receiver. Moreover, this receiver can cope with the sensitivity of larger constellations in general non-uniform constellations in particular to ISI introduced by a severely frequency dispersive channels as shown in the performance results.

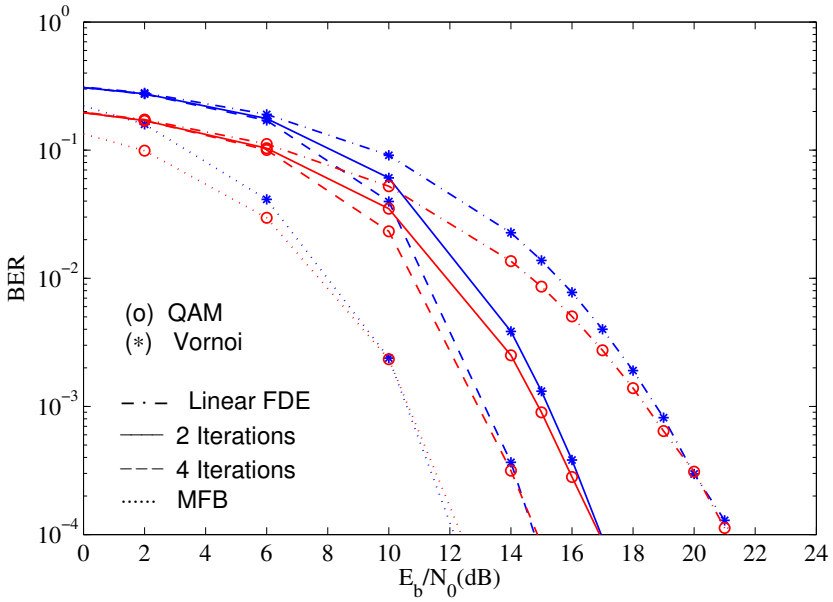

Figure 4.14: Performance results for 16-QAM and Voronoi optimized constellations over fading channel

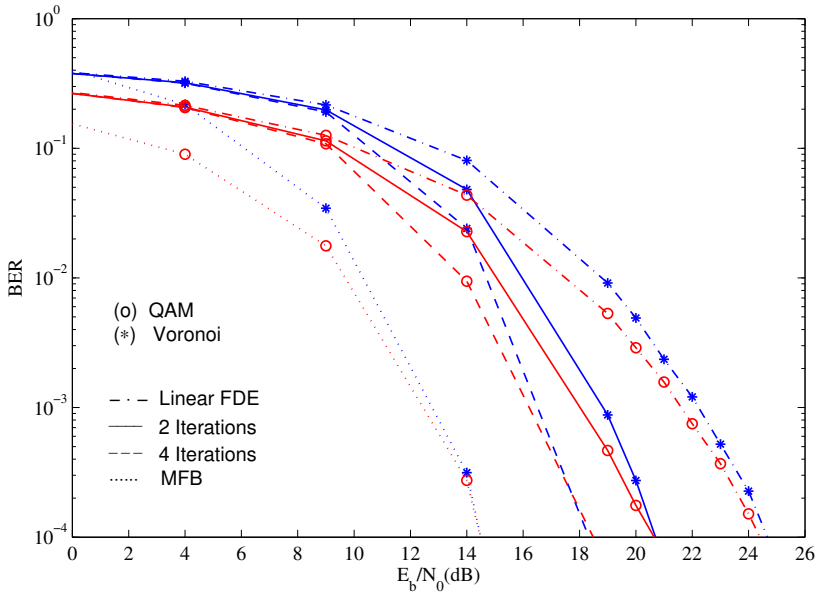

Figure 4.15: Performance results for 32-QAM and Voronoi optimized constellations over fading channel

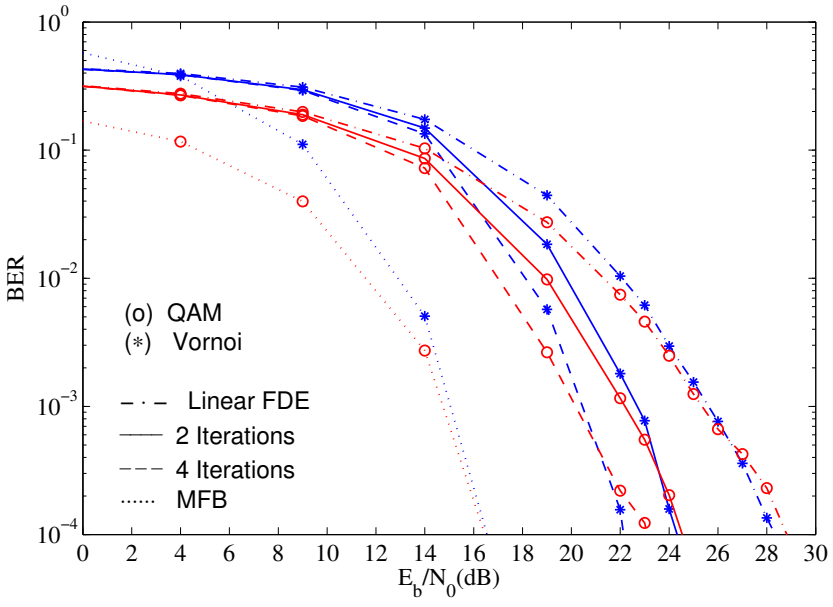

Figure 4.16: Performance results for 64-QAM and Voronoi optimized constellations over fading channel

Non-Uniform Gain and Phase Imbalance Performance

The bigger drawback in this transmitter is the phase and gain imbalances along the amplifiers, leading to a non-uniform constellations output. In this section we are going to analyse the non-uniform phase and gain unbalance consequences in the system performance, taking into account the transmitter described in the last chapter. we assumed the SC-FDE modulation and the time-dispersive channel used in the previous section. Any phase imbalance after the amplifier is ignored.

Is depicted at Figure 4.17, 4.18, 4.19 and 4.20 the BER performance results with 16-QAM and Voronoi for phase and gain imbalances. Clearly the performance improves with the number of iteration as we have seen at the system with the perfect synchronization. Denote at Fig.4.18 and Fig.4.20 for $\sigma = 5^{o}$ and $\Delta G = 0.1$ respectively and values of E_n/N_0 higher than 20dB we have some error propagation at the iterative process. The iterative process suffers from error propagation, i.e. it is recovering the original signal till some energy value, and then deteriorates the signal because it cannot compensate. Increasing the energy will not provide a better BER performance because for values higher that 20db we are having worst performance.

The conclusions of last chapter about phase and gain imbalances through an AWGN channel are still valid for a frequency dispersive channel. The performance of 32 and 64 Voronoi and QAM constellation can be seen in Appendix A

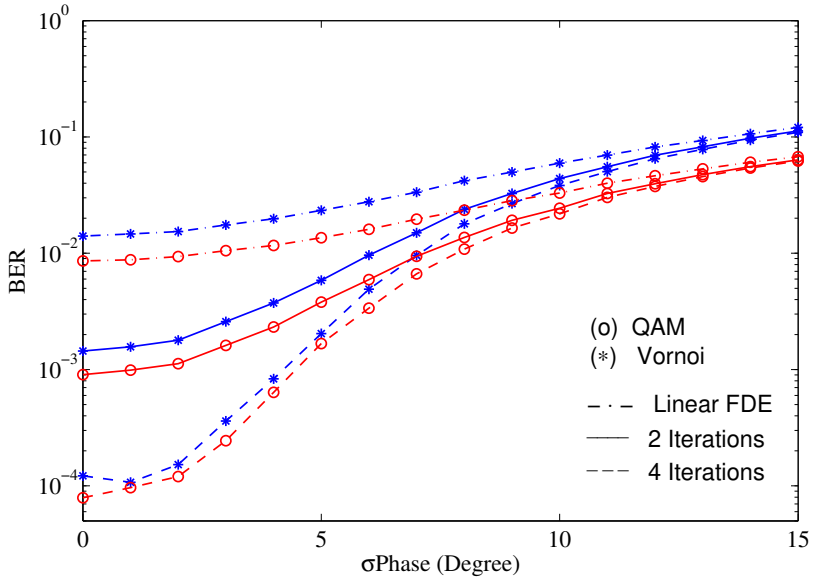

Figure 4.17: Performance results for 16-QAM and Voronoi over fading channel with $E_b = 15$ dB for continuous phase imbalances

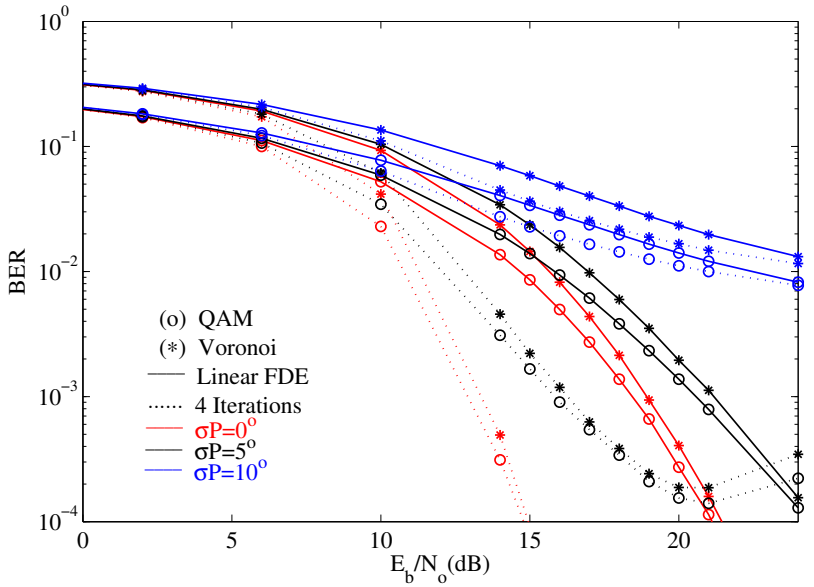

Figure 4.18: BER performance results for 16-QAM and Voronoi over fading channel with phase imbalances of 0, 5 and 10 degrees

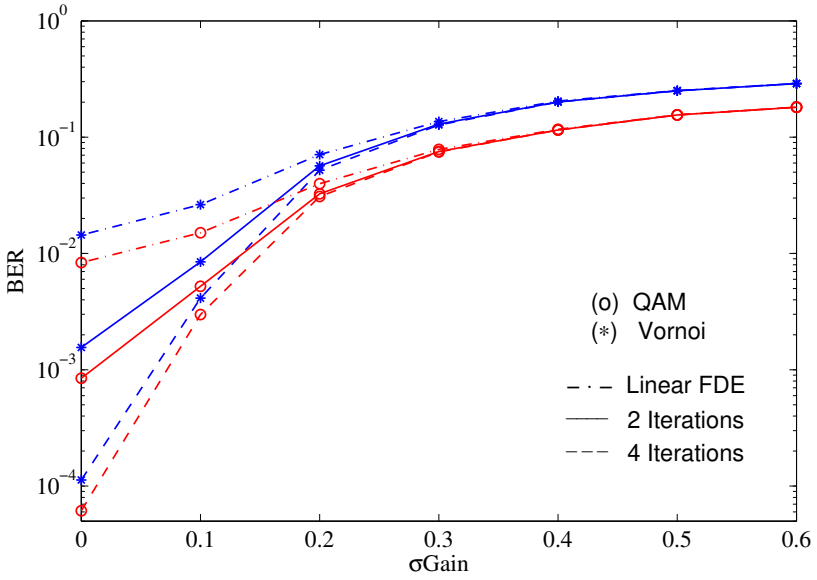

Figure 4.19: Performance results for 16-QAM and Voronoi over fading channel with $E_b =$ 15 dB for continuous gain imbalances

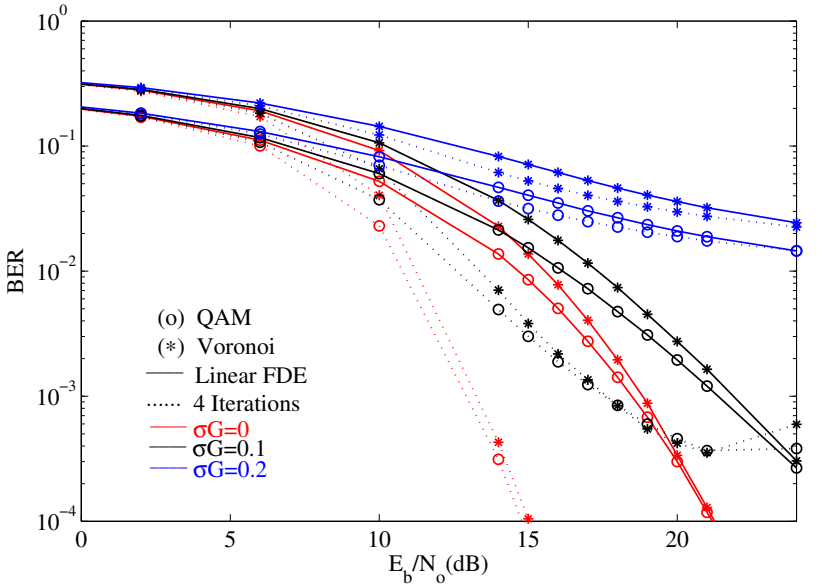

Figure 4.20: BER performance results for 16-QAM and Voronoi over fading channel with gain imbalances of 0, 0.1 and 0.2

5

Conclusions and Future Work

5.1 Conclusions

In the wireless systems the biggest energy consumption is at the transmitter amplifiers. The minimization of the transmitted energy would enable a significant increase in the power efficiency of the wireless mobile devices, leading to a systems were the time interval between battery charges is significantly increased. This improvement seems to be not so important when we have power supply everywhere, but thinking about some countries with lack of energy and military communications where the mobile systems autonomy is crucial it can make a big difference.

In chapter 2 were introduced a constellations design and optimization in order to increase the spectral efficiency without sacrificing the energy efficiency. Some parameters as number of adjacent symbols, PAPR and the energy gains of each constellation have been taking into account in the way to analyse the constellations efficiency.

Voronoi constellations have higher energy gains comparing with the QAM, for the same constellations size. As mentioned these gains are associated to a higher number of adjacent symbols, which can compromise the performance for low SNR. The non-uniform Voronoi constellations do not have a regular shape. Consequently the decisions regions are irregulars, this fact can have impact in the receiver's complexity

Signals with lower PAPR are less sensitive to non linear amplifier effects. Therefore we could see that Voronoi ensure better PAPR ratio with lower energy than Square-QAM constellations.

Based on the constellations decomposition as a sum of BPSK sub-constellations, it is possible to write the constellations symbols as a linear function of the transmitted bits. This method was then employed to design the iterative receiver that can cope with any kind of constellation.

Chapter 3 presented an amplification technique using non-linear amplifiers for generic multidimensional constellations based on BPSK sub-constellations decomposing. The non-linear amplifiers have bigger efficiency but must be employed only for signals with low envelope fluctuation.

MSK modulations scheme can be seen as a OQPSK signal where the modulation pulse is half cosine instead of rectangular pulse. This modulation pulse change creates a constant envelope signal that can be amplified by non-linear devices.

When we shift the reference carrier as shown in section 3.1 a parallel OQPSK stream can be seen as a BPSK serial bit stream where even and odd bits are respectively in-phase and quadrature bits. Extending the OQPSK parallel to serial propriety to these sub-constellations and shifting the carrier frequency we have a stream with each symbol represented by two samples, the T and T+1 samples represent the in-phase and quadrature components of the signal respectively. Due to the asymmetrical constructions and synchronization, the parallel amplification has some phase and gain imbalances causing distortion of the resultant constellations and compromising the system performance. As expected the system performance decrease with the phase and gain imbalances.

In Chapter 4 were introduced the basic principles of SC modulations. It was shown that block transition schemes including CP and FFT algorithms are very efficient and allows receivers with low complexity. The performance of SC-FDE systems is similar to an OFDM, however there is a significant difference: the decision about the transmitted bits in the SC-FDE is performed in the time domain.

IB-DFE is an iterative DFE for SC-FDE where feedback and feedforward filters are implemented in the frequency-domain. By cancelling the residual interference in each iteration, the performance benefits obtained are very significant. Replacing the "hard-decisions" by

"soft-decisions" and taking advantage from the decomposition of constellations on BPSK components, we can design a receiver able to deal with any constellation without requiring a significant increase in system complexity. This method is then employed to design iterative receivers, implemented in the frequency-domain, that can cope with higher sensitivity to ISI effects of the resultant constellations from the energy optimization.

5.2 Future Work

In the scope of the future work, we emphasis those aspects that aim to improve the actual system. These improvements aim to reduce the system complexity, implementation architecture and some extra techniques to improve the system performance:

- Development of techniques for estimating the unbalance between amplifiers
- Receiver design taking into account the unbalance between amplifiers
- Extension of these techniques for offset modulations
- Extension of these techniques to multi-dimensional constellations with good power/bandwidth trade-off [33]
- Design of good coded modulation schemes

Bibliography

[1] C. P. Liang, J. H. Jong, W. E. Stark, and J. R. East, "Nonlinear Amplifier Effects in Communications Systems," *IEEE Transactions Microwave Theory Technology*, vol. 47, pp. 1461–1466, 1999.

[2] J. G. Proakis, *Digital Communications*. McGraw-Hill, 1995.

[3] H. Sari, G. Karam, and I. Jeanclaude, "An analysis of Orthogonal Frequency-Division Multiplexing for Mobile Radio Applications," no. 1, pp. 1635–1639, 1994.

[4] A. Gusmao, R. Dinis, J. Conceicão, and N. Esteves, "Comparison of Two Modulation Choices for Broadband Wireless Communications," *Vehicular Technology Conference Proceedings, IEEE VTC 2000-Spring Tokyo*, vol. 2, pp. 1300–1305 vol.2, 2000.

[5] S. L. Ariyavisitakul, B. Eidson, and D. Falconer, "White Paper: Frequency Domain Equalization for Single-Carrier Broadband Wireless Systems," *IEEE Communication Mag*, vol. 40, pp. 58–66, 2002.

[6] N. Benvenuto and S. Tomasin, "Block Iterative DFE for Single Carrier Modulation," *IEEE Electronics Letters*, vol. 38, no. 19, pp. 1144–1145, 2002.

[7] R. Dinis, A. Gusmao, and N. Esteves, "On Broadband Block Transmission over Strongly Frequency-Selective Fading Channels," *IEEE Wireless*, pp. 261–269, July 2003.

[8] R. Dinis, A. Gusmao, and N. Esteves, "Iterative Block-DFE Techniques for Single-Carrier-Based Broadband Communications with Transmit/Receive Space Diversity," in *Wireless Communication Systems, 2004, 1st International Symposium on*, sept. 2004, pp. 347 – 351.

[9] R. Dinis, R. Kalbasi, D. Falconer, and A. Banihashemi, "Iterative Layered Space-Time Receivers for Single-Carrier Transmission over Severe Time-Dispersive Channels," *IEEE Communication Letters*, vol. 8, pp. 579–581, September 2004.

[10] Benvenuto, Nevio and Tomasin, Stefano, "Iterative design and detection of a dfe in the frequency domain." *IEEE Transactions on Communications*, vol. 53, no. 11, pp. 1867–1875, 2005.

[11] A. Gusmao, P. Torres, D. R., and E. N., "A Class of Iterative FDE Techniques for Reduced-CP SC-Based Block Transmission," *Int. Symposium on Turbo Codes*, pp. 1–6, April 2006.

[12] A. Gusmao, P. Torres, R. Dinis, and N. Esteves, "A Turbo FDE Technique for Reduced-CP SC-Based Block Transmission Systems," *IEEE Transactions on Communications*, vol. 55, no. 1, pp. 16–20, 2007.

[13] J. Smith, "Odd-bit Quadrature Amplitude-Shift Keying," *IEEE Transactions on Communications*, vol. COM-23, no. 3, pp. 385–389, March 975.

[14] S. Haykin, *Communication Systems*, 5th ed. Wiley Publishing, 2009.

[15] H. Yu and G. Wei, "Symbol Error Probability of Cross QAM in Rayleigh Fading Channels," *Commmunication Letters.*, vol. 14, no. 5, pp. 375–377, May 2010.

[16] J. Forney, G.D., "Coset Codes. I. Introduction and Geometrical Classification," *Information Theory, IEEE Transactions on*, vol. 34, no. 5, pp. 1123 –1151, sep 1988.

[17] J. Forney, G.D. and L.-F. Wei, "Multidimensional Constellations. I. Introduction, Figures of Merit, and Meneralized Cross Constellations," *Selected Areas in Communications, IEEE Journal on*, vol. 7, no. 6, pp. 877 –892, aug 1989.

[18] A. Calderbank and L. Ozarow, "Nonequiprobable Signaling on the Gaussian Channel," *Information Theory, IEEE Transactions on*, vol. 36, no. 4, pp. 726 –740, jul 1990.

[19] G. Foschini, R. Gitlin, and S. Weinstein, "Optimization of Two-Dimensional Signal Constellations in the Presence of Gaussian Noise," *Communications, IEEE Transactions on*, vol. 22, no. 1, pp. 28 – 38, jan 1974.

[20] F. Pfender and G. M. Ziegler, "Kissing Numbers, Sphere Packings and some Unexpected Proofs," *Notices American Mathematical Society*, vol. 51, pp. 873–883, 2004.

[21] G. J. Forney, R. Gallager, G. Lang, F. Longstaff, and S. Qureshi, "Efficient Modulation for Band-Limited Channels," *Selected Areas in Communications, IEEE Journal on*, vol. 2, no. 5, pp. 632–647, 1984.

[22] J. M. Cioffi, "Data Transmission Theory," course Text from EE379A chap.1.

[23] P. Montezuma and A. Gusmao, "On Analytically Described Trellis-Coded Modulation Schemes," *ISCTA'01*, July 2001.

[24] Miguel Luzio, Rui Dinis, Paulo Montezuma, Vitor Astucia and Marko Beko, "Efficient Receivers for SC-FDE with Offset Modulations," *IEEE Milcom 2012, Orlando, USA*, 2012.

[25] S. Pasupathy, "Minimum Shift Keying: A Spectrally Efficient Modulation," *Communications Magazine, IEEE*, vol. 17, no. 4, pp. 14–22, 1979.

[26] F. Amoroso and J. Kivett, "Simplified MSK Signaling Technique," *IEEE Transactions Communicattions*, vol. COM-25, pp. 433–441, April 1977.

[27] S. Pupolin and L. J. Greenstein, "Performance Analysis of Digital Radio Links with Nonlinear Transmit Amplifiers," *IEEE Journal of Selected Areas in Communications*, vol. 5, pp. 535–546, 1987.

[28] A. Georgiadis, "Gain, phase imbalance, and phase noise effects on error vector magnitude," *Vehicular Technology, IEEE Transactions on*, vol. 53, no. 2, pp. 443 – 449, march 2004.

[29] Z. Zhu, X. Huang, and M. Caron, "Analytical Performance of M-PSK Communications Systems in the Presence of Gain/Phase Imbalances and DC-Offsets," *Wireless Communications Letters, IEEE*, vol. 1, no. 4, pp. 404 –407, august 2012.

[30] J. Proakis and D. Manolakis, *Digital Signal Processing*. Pearson Prentice Hall, 2007.

[31] A. Czylwik, "Comparison Between Adaptive OFDM and Single Carrier Modulation with Frequency Domain Equalization," *Simulation*, vol. 2, pp. 865–869, 1997.

[32] R. Dinis, P. Montezuma, N. Souto, and J. Silva, "Iterative Frequency-Domain Equalization for General Constellations," in *Proceedings of the 33rd IEEE Conference on Sarnoff*, ser. Sarnoff'10. Piscataway, NJ, USA: IEEE Press, 2010, pp. 137–141.

[33] M. Beko and R. Dinis, "Designing Good Multi-Dimensional Constellations," *Wireless Communications Letters, IEEE*, vol. 1, no. 3, pp. 221 –224, june 2012.

A

Appendix

A.1 Phase Imbalances

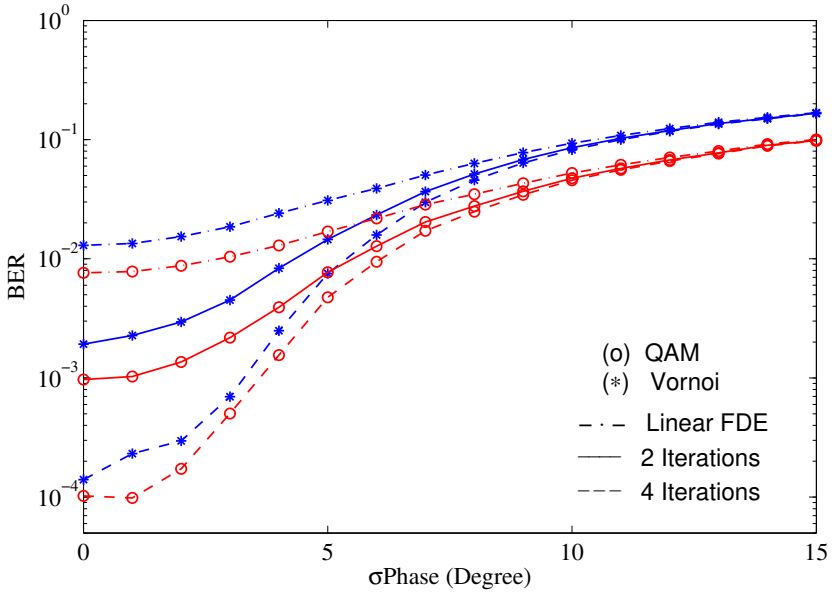

Figure A.1: Performance results for 32-QAM and Voronoi over fading channel with $E_b =$ 18 dB for continuous phase imbalances

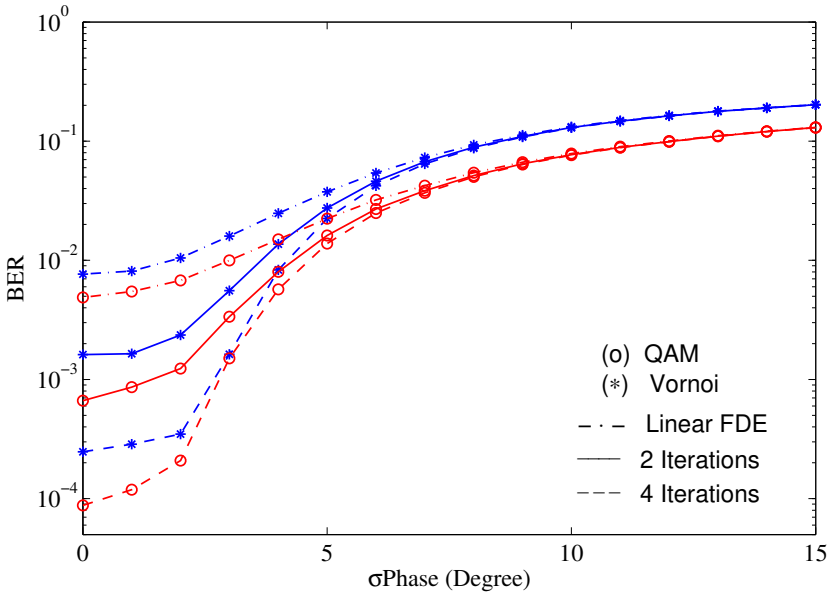

Figure A.2: Performance results for 64-QAM and Voronoi over fading channel with $E_b =$ 22 dB for continuous phase imbalances

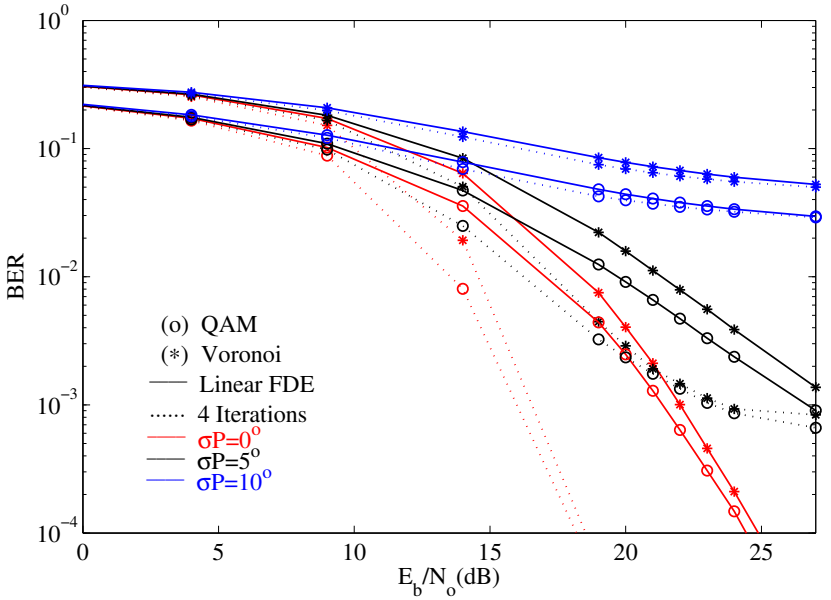

Figure A.3: BER performance results for 32-QAM and Voronoi over fading channel with phase imbalances of 0, 5 and 10 degrees

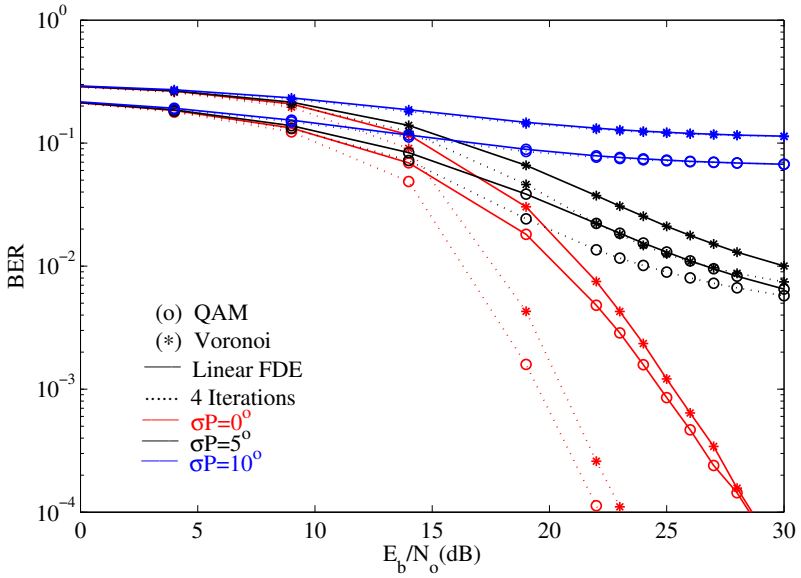

Figure A.4: BER performance results for 64-QAM and Voronoi over fading channel with phase imbalances of 0, 5 and 10 degrees

A.2 Gain Imbalances

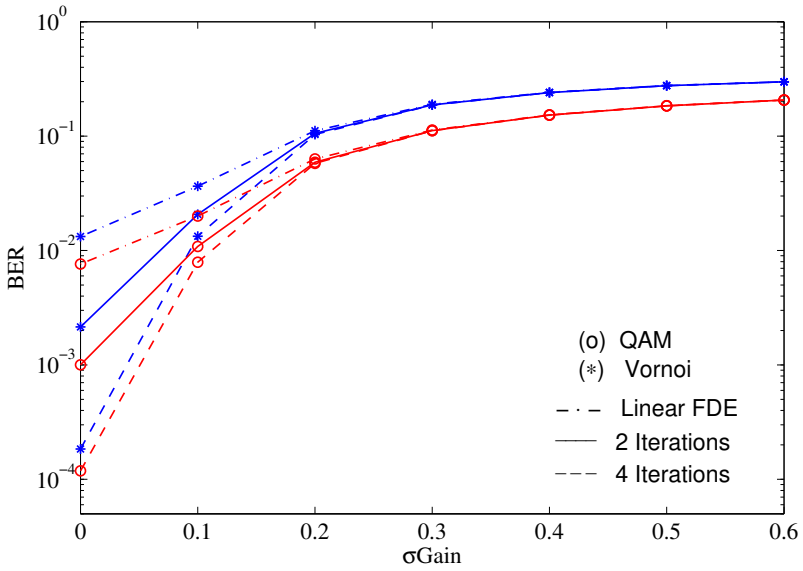

Figure A.5: Performance results for 32-QAM and Voronoi over fading channel with $E_b =$ 18 dB for continuous gain imbalances

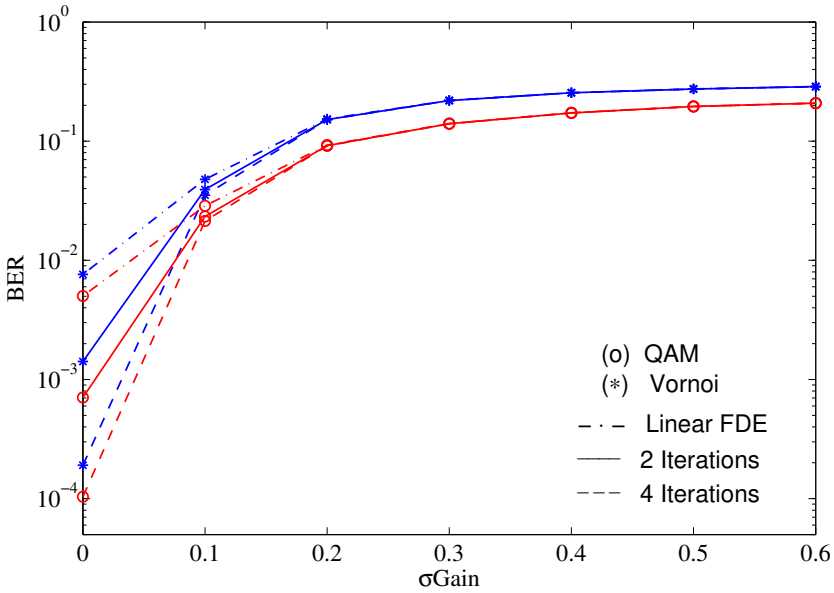

Figure A.6: Performance results for 64-QAM and Voronoi over fading channel with $E_b =$ 22 dB for continuous gain imbalances

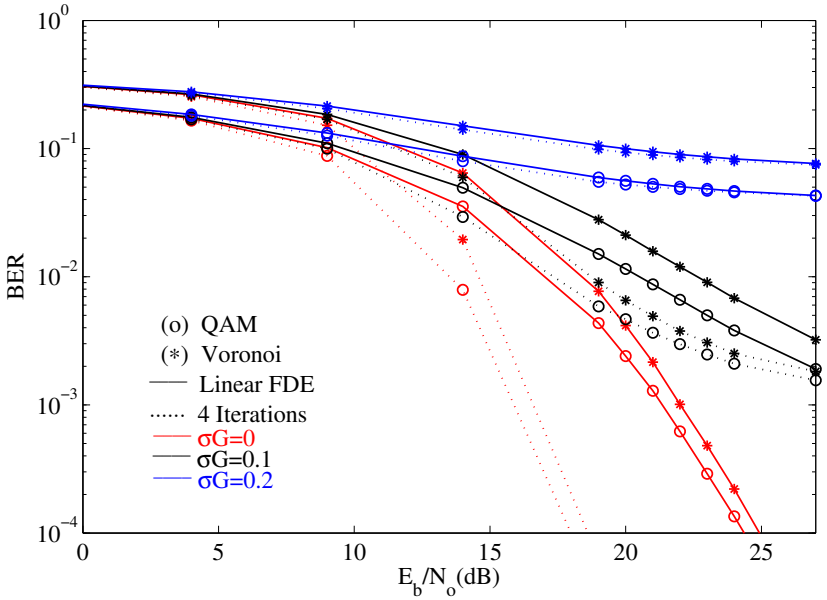

Figure A.7: BER performance results for 32-QAM and Voronoi over fading channel with gain imbalances of 0, 0.1 and 0.2

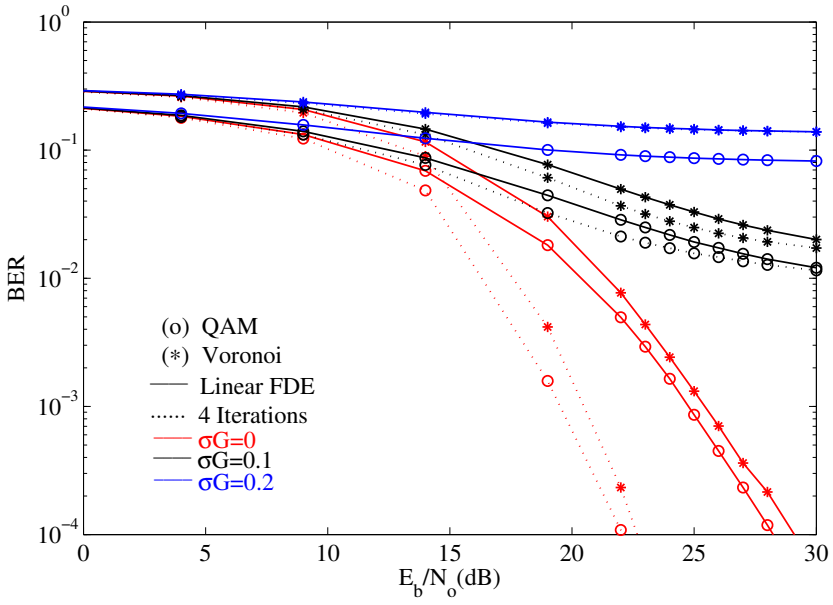

Figure A.8: BER performance results for 64-QAM and Voronoi over fading channel with gain imbalances of 0, 0.1 and 0.2